NOVA SCHOOL OF SCIENCE & TECHNOLOGY

DEPARTMENT OF ELECTRICAL AND COMPUTER ENGINEERING

CATARINA RODRIGUES NOGUEIRA

BSc in Electrical and Computer Engineering Sciences

WIRELESS POWER TRANSFER WITH SUPERCONDUCTING COILS

MASTER IN ELECTRICAL AND COMPUTER ENGINEERING

NOVA University Lisbon
September, 2022

NOVA SCHOOL OF SCIENCE & TECHNOLOGY

DEPARTMENT OF ELECTRICAL AND COMPUTER ENGINEERING

WIRELESS POWER TRANSFER WITH SUPERCONDUCTING COILS

CATARINA RODRIGUES NOGUEIRA

BSc in Electrical and Computer Engineering Sciences

Adviser: João Miguel Murta Pina
Full Professor, NOVA University Lisbon

Co-adviser: Luís Filipe Romba Jorge
MSc, NOVA University Lisbon

Examination Committee

Chair: Name of the committee chairperson
Full Professor, FCT-NOVA

Rapporteur: Name of a rapporteur
Associate Professor, Another University

Members: Another member of the committee
Full Professor, Another University

Yet another member of the committee
Assistant Professor, Another University

MASTER IN ELECTRICAL AND COMPUTER ENGINEERING

NOVA University Lisbon
September, 2022

Wireless Power Transfer with Superconducting Coils

This document was created with the (pdf/Xe/Lua)LaTeX processor and the NOVAthesis template (v6.9.15) Lourenço, 2021.

Acknowledgements

In this section I would like to express my thanks to all those who contributed to the accomplishment of this work and for the academic journey.

I want, firstly, to thank my adviser, Prof. Dr. João Murta Pina, for giving me the opportunity to develop this dissertation. The possibility that was given to me, allowed me to evolve as a person and as an academic.

To my co-adviser, MSc Luís Romba Jorge, a special thanks. For all the availability, support and dedication. Throughout this year of work, directed to the development of this dissertation, many were the meetings and help in the laboratory in order to achieve its success.

To Marcelo and Jodu for all the support and friendship that you gave throughout these years. For all the endless hours spent at 7 and in the library "studying". For all the companionship and much more that I will carry with me forever.

To Ulisses, for all the conversations about infinite different topics, which so often make me smile when I least feel like it. For the friendship that has grown from year to year, and that I will certainly take with me for the rest of my life. For everything you've taught me and continue to teach, when I grow up, I'll be happy if I'm half the person you are.

To Pinto, for being with me since the beginning of this journey. For the support, friendship and for all the good and bad times. For the respect, affection and concern that you have always had and that characterise you so much. For these years and for the many more that I know will come, because a friendship like this just came to stay forever.

A very special thanks to Francisco, for everything you mean to me and for being the best that college has given me. The patience you had with me during the realisation of this work, when I was desperate because nothing worked, was crucial for me to reach the end. I thank you for the motivation you always gave me throughout these years of faculty and for being by my side when everything was going wrong.

Finally, I would like to thank my family, especially my parents and grandparents, who have always been there for me, by giving me support during this journey. A warm thanks to my parents for all the help and sustenance, without which I would never have been able to pursue this dream of mine.

To all of you,
My heartfelt and sincere thank you!

"Even the smallest person can change the course of the future." (Galadriel)

Abstract

With the growing need for electrical systems that make life easier for the user, interest has arisen for contactless power transfer systems that allow no cables to exist and to transfer energy over considerable distances. However, the efficiency of these systems decreases considerably when the distance between the receiving coil and the transmitter is increased due to a considerable increase in system losses.

High temperature superconducting materials have increasing potential in energy applications due to their characteristics, namely virtually zero dc resistance, and the fact that they have been discovered to be cooled with liquid nitrogen. Due to the reduction in the efficiency of energy transfer systems without contact with the increased distance between the receiver and the transmitter, it is necessary to study these systems with the replacement of copper coils by superconducting tape coils in order to understand whether it is possible to have considerable efficiency at greater distances.

This study is the basis of this dissertation, whose main objective is the construction of a functional prototype of energy transfer without contact with superconducting coils for charging an acid-lead battery. First, we present the study of a power supply with rectification, filtration, voltage regulation, and current limitation in order to ensure the correct charging of the battery.

Secondly, the implemented contactless energy transfer system consisting of two superconducting tape coils is described.

In all the work performed, one of the guidelines in the creation of the prototype was the use of simulation tools of the system, namely MATLAB/Simulink in order to understand the functioning of each component that composes it before performing the experimental part.

Keywords: Wireless Power Transfer, High-Temperature Superconducting Coils, Lead-Acid Battery, Power Supply

Resumo

Com a crescente necessidade por sistemas elétricos que facilitam a vida do utilizador, surgiu o interesse por sistemas de transferência de energia sem contacto que permitem que não existam cabos e que se possa transferir energia por distâncias consideráveis. No entanto, a eficiência destes sistemas diminui consideravelmente quando se aumenta a distância entre a bobina recetora e a transmissora, devido a um aumento considerável das perdas do sistema.

Os materiais supercondutores de alta temperatura têm um crescente potencial em aplicações na área da Energia devido às suas características, nomeadamente resistência virtualmente nula em DC, e ao facto de se ter descoberto que podem ser arrefecidos com azoto líquido. Devido à redução da eficiência dos sistemas de transferência de energia sem contacto com o aumento da distância entre o recetor e o transmissor, torna-se necessário o estudo destes sistemas com a substituição das bobinas de cobre por bobinas de fita supercondutora por forma a se compreender se é possível se ter uma eficiência considerável a maiores distâncias.

Esse estudo é a base da presente dissertação, que tem como principal objetivo a construção de um protótipo funcional de transferência de energia sem contacto com bobinas supercondutoras para carregamento de uma bateria de ácido-chumbo. Em primeiro lugar, apresenta-se o estudo de uma fonte de alimentação com retificação, filtragem, regulação de tensão e limitação de corrente por forma a se garantir o correto carregamento da bateria.

Em segundo lugar, descreve-se o sistema de transferência de energia sem contacto implementado composto por duas bobinas de fita supercondutora.

Em todo o trabalho, uma das linhas orientadoras na criação do protótipo foi a utilização de ferramentas de simulação do sistema, nomeadamente MATLAB/Simulink por forma a se entender o funcionamento de cada componente que o compõem antes de se efetuar a parte experimental.

Palavras-chave: Transmissão de Energia sem Contacto, Bobinas Supercondutoras de Alta Temperatura, Bateria de Ácido de Chumbo, Fonte de Alimentação

Contents

List of Figures

List of Tables

Acronyms

AC Alternating Current. *(p. 17)*

BCS Bardeen–Cooper–Schrieffer. *(p. 14)*
BSCCO Bismuth-Strontium-Calcium-Copper-Oxide. *(p. 15)*

DC Direct Current. *(p. 17)*

GDSCC Goldstone Deep Space Communications Complex. *(p. 8)*

HTS High-Temperature Superconductors. *(p. 14)*

JPL Jet Propulsion Laboratory. *(p. 8)*

MIT Massachusetts Institute of Technology. *(p. 8)*

NASA National Aeronautics and Space Administration. *(p. 8)*

RF Radio Frequency. *(p. 8)*

SHARP Stationary High-Altitude Relay Platform. *(p. 8)*
SPS Solar Power Satellite. *(p. 8)*

WPT Wireless Power Transfer. *(pp. 6–8, 10, 15, 16, 19)*
WSN Wireless Sensor Networks. *(p. 11)*

YBCO Yttrium-Barium-Copper-Oxide. *(p. 15)*

Symbols

A	Exponential zone amplitude ($(Ah)^{-1}$).
B	Magnetic induction field intensity or magnetic flux density (T).
C	Electrical capacity (F).
C_1	Electrical capacity of the emitter's capacitor (F).
d	Distance between the transmitter and receiver coils (cm).
E	No-load voltage (V).
E_0	Battery constant voltage (V).
f	Frequency (Hz).
f_r	Resonant frequency (Hz).
i	Battery current (A).
I	Electrical current (A).
I_1	Electrical current of the emitter circuit (A).
I_2	Electrical current of the receiver circuit (A).
k_{12}	Coupling factor between the receiving and transmitting coils.
K	Polarisation voltage (V).
L	Self-induction coefficient (H).
L_1	Self-induction coefficient of the emitter coil (H).
L_2	Self-induction coefficient of the receiver coil (H).
M_{12}	Mutual inductance between the receiving and transmitting coils.

Q Quality factor.
Q_{batt} Battery capacity (Ah).

R Electrical resistance (Ω).
R_{int} Battery internal resistance (Ω).
R_L Electrical load resistance (Ω).
R_s Electrical source resistance (Ω).

U_{OC} Open-circuit voltage (V).

V_{batt} Battery voltage (V).
V_{ind} Voltage induced in the receiver coil (V).
V_r Ripple voltage (V).
V_s Source voltage (V).

η Efficiency.

μ_0 Magnetic void permeability ($4\pi \times 10^{-7}$ H/m).

ω Angular frequency (rad/s).

1

Introduction

This chapter contextualises the problem on which this dissertation focuses, as well as the motivation and efforts made to date to solve it. Efforts in the area focus mainly on improving contactless energy transfer systems. In addition, the existence of relevant studies in the evaluation and characterization of existing technology allows a constant development in the path of a better efficiency of the same.

The motivation for the dissertation is the initial section of this introductory chapter, demonstrating what led to the study of these systems and adjacent problems. The following section shows the research questions that have arisen and the hypotheses of answer. Section 1.3 refers to the objectives of the work to be developed in this project. The following section refers to the main contributions that the developed project has made to the work carried out previously. Finally, the last section presents the structure of this document.

1.1 Motivation

Nowadays, it's not possible to imagine a day passing without electricity. It is not needed to light our houses and allow us to cook, clean and charge our cell phones and laptops. But it also involves the support of a lot of different industries, such as the technology one. This industry has brought to us electric cars that are one of the solutions to a problem that humankind is now facing: climate change. Fossil fuel-based transportation has revolutionised mobility over the past century, catalysing modernization while at the same time contributing to the biggest challenge of our time. With the emission of carbon dioxide there was the need to change our cars fuel and so electricity came into the picture.

Due to the growing need for electric cars came the need for better storage solutions and therefore bigger batteries. With bigger batteries, the need for faster charging appears. Normally when charging a battery, whether of an electric car or of a cell phone, cables are used. However, using cables can be very hazardous and inconvenient. Because of this, wireless power transfer has become an increasingly interesting solution that allows the transfer of energy without any cables.

Nevertheless, wireless power transfer has its problems, being that the biggest one is its low efficiency with increasing distances between the transmitter and receiver. In order to try to reduce this problem, the main motivation of this dissertation will be on the use of high-temperature superconductors, which, despite their ceramic character, are likely to be liquid nitrogen cooled, a relatively inexpensive cryogenic liquid with abundant commercial availability.

1.2 Research Question and Hypothesis

1.2.1 Research Questions

The main research questions chosen to guide this work are the following:

Q1 – How to improve the efficiency of a wireless power transfer system for distances of several centimetres between the receiving and transmitting coils?

Q2 – Can superconducting coils be used in a wireless power transfer system with frequencies of kHz and not lose its superconducting properties?

Q3 – How to create a power supply system with voltage regulation and current limit as the output unit of the wireless power transfer system to charge a battery?

1.2.2 Hypothesis and Approaches

Proposed hypotheses to address the research questions are:

H1 – Due to the virtual zero resistance in DC, which means no losses in DC, superconducting coils can be used to increase the efficiency of a wireless power transfer system for considerable distances between the two coils.

H2 – In AC as the frequency increases so does the current and with that the temperature of the coils also increases which if it increases too much the coils could leave its superconducting state, so to avoid this there needs to be a compromise between the necessary current to have a functional WPT system and the current that can maintain the superconducting state of the coils.

H3 – Simulation models for power supplies can be developed based on its several components, which will allow it to consider and evaluate its performance when maintaining a certain output voltage and current.

1.3 Objectives

In view of the mentioned previously, the main objective of this dissertation is to evaluate the practicality of contactless energy transfer systems based on superconducting coils for charging batteries in magnetic levitation trains (maglev). This means verifying if the efficiency of the referred systems is acceptable through the reduction of losses with the use of superconducting coils.

Thus, the inherent objectives are the study of the charging of a battery, to understand its operation and how wireless energy transfer is used in this application, and the study of the contactless energy transfer system with superconducting tape coils instead of the usual copper coils, so that its feasibility can be evaluated. To do so, it is necessary to simulate the entire system, including the electronic converters and the batteries that, onboard the maglev, will allow the storage of the transferred energy.

This study will consist of the simulation of the system in MATLAB/Simulink and the construction of a functional prototype of the wireless power transfer system with a power supply as the output unit of the system.

1.4 Main Contributions

This work contributes to improving the study of power transfer systems without contact with superconducting coils in the transmitter and receiver circuits for the charging of a battery. This contribution is structured by analysing the main components that make up this system, including a power supply as the output unit of the receiver circuit placed before the battery.

It is shown in this work that the use of simulation tools such as MATLAB/Simulink before the construction of the prototype is possible to have a prediction of what would be the behaviour of the system built in laboratory tests.

It is also indicated in this work the process of construction of a functional prototype of the contactless energy transfer system, in which it was possible to observe that this system has a decay of mutual inductance close to an exponential as the distance between the coils is increased.

1.5 Dissertation Organisation

In order to fulfil the proposed objectives, this dissertation is divided into six chapters. The initial chapter presents the motivation for the work carried out and the objectives that were intended to be achieved. The remaining chapters are directly related to the work that was developed.

In the second chapter, called “State of the Art”, a survey is made of the history and practical evolution of contactless energy transfer systems. The same is done with regard to superconductivity and the main characteristics of these materials, with special emphasis on the superconducting tape. Reference is made to the main constituents of a power supply.

In the third chapter, the methodology related to the design of a power supply and a contactless energy transfer system are discussed. As far as contactless energy transfer is concerned, they are the coupling factor between the two coils, the mutual inductance coefficient, and the efficiency of these systems.

The fourth chapter describes the procedure for simulating the power supply and contactless energy transfer. The experimental procedure used to perform the various measurements necessary to answer the questions that were initially stated is also described, and the results obtained are presented.

The fifth chapter presents the analysis and interpretation of the results obtained by simulation and experimentally with the created prototype.

In the last chapter, the conclusions of the work are presented and future work is suggested that will allow us to extend what was started with this dissertation.

2

State of the Art

Through the next sections, the state of the art of the present dissertation will be presented, being structured as:

2.1. Wireless Power Transfer: This starts with a historical review of the discovery and development of contactless energy transfer. The section follows with the description of the techniques of non-contact energy transfer, necessary to better understand the operation of these systems. It concludes with the presentation of the different compensation topologies.

2.2. Superconductive Materials: Begins with a review of the discovery and history of superconductivity. The section concludes with the description of tape superconductors inserted into high-temperature superconductors.

2.3 Wireless Power Transfer with Conventional Coils *Versus* Superconducting Coils: Explains the advantages of using superconducting coils in systems of wireless power transfer instead of the usual copper coils.

2.4 Power Supply: Describes the various components of a power supply system, which constitutes the output unit of the energy transfer system.

2.1 Wireless Power Transfer

2.1.1 Introduction and History Perspective

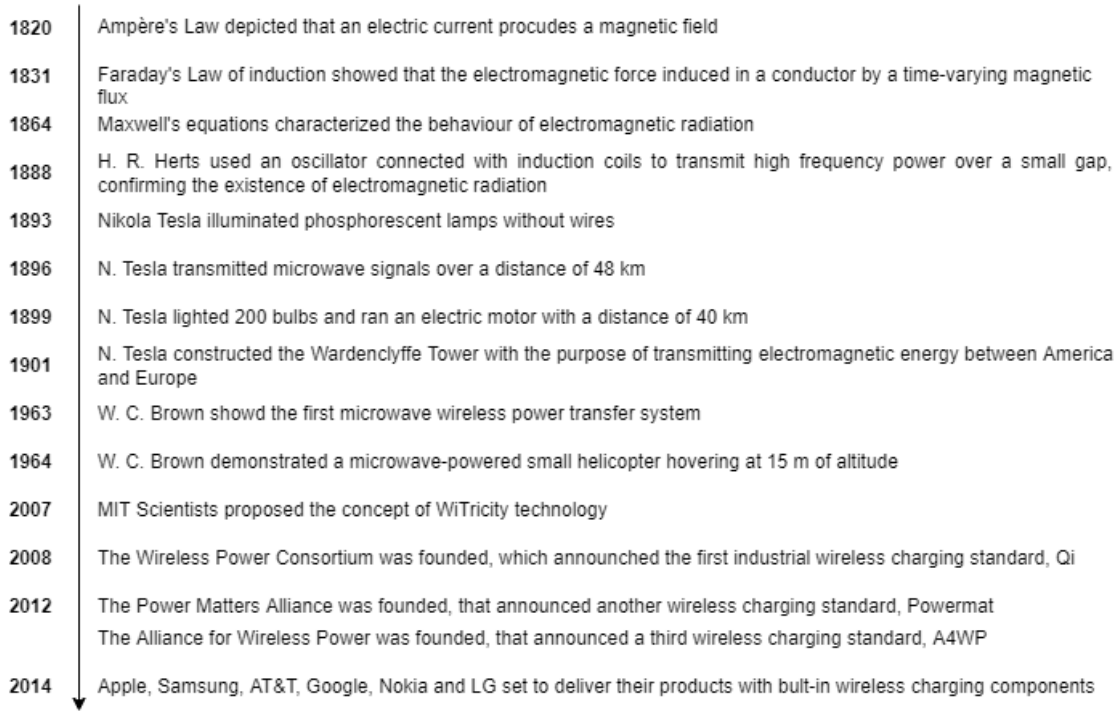

Figure 2.1: Wireless Power Transfer's brief history (Lu et al., 2015; Lu et al., 2016).

The history of Wireless Power Transfer (WPT) starts in 1891 when Nikola Tesla, best known for being the founder of alternating current electrical energy, first conjured the concept of Wireless Power Transmission and showed that the transfer of electrical energy without the use of cables depends on electrical conductivity (Mohammed et al., 2010). In the same year, he created a type of resonant transformer, which was named the Tesla Coil, that had the objective of creating electrical energy with a large voltage, small current and high frequency (Bhutkar & Sapre, 2009).

Then in 1893, Tesla showed the lighting of vacuum bulbs free from cables for the transfer of power at the World Columbian Exposition in Chicago (Mohammed et al., 2010; Singh et al., 2012). In 1896, he focused his work on WPT with long distances and produced the transfer of microwave signals through 48 km (Lu et al., 2016). Later in 1899, he was capable of transmitting 10 million Volts of electrical high-frequency power with 40,23 km of distance to illuminate 200 bulbs and operate an electric motor (Lu et al., 2015). He claimed to have achieved a 95% of efficiency and used the employment of the planet's resonance with its particular vibrational frequency to conduct alternating electric current across a large electric oscillator at 7,8 Hz (Bhutkar & Sapre, 2009).

In 1901, Tesla manufactured a tower named Wardenclyffe Tower with the purpose of transfering electrical energy globally without wires through the Ionosphere. Nevertheless, because of the limitations of the technology, for example, the low efficiency of the system, the idea hasn't been extensively developed and commercialized (Lu et al., 2015).

Figure 2.2: The 57 meters tall Wardenclyffe Tower (Mohammed et al., 2010).

The discovery of WPT was conditioned by the study and understanding of the principle of electromagnetism, which began in 1819 when H. C. Ørsted found out that an electric current creates a magnetic field around it. From this study came three important laws: Ampère's Circuital Law, Biot-Savart's Law and Faraday's Law. The first one describes the magnetic field that is integrated around a closed loop to the electric current passing through the loop. The second characterizes the magnetic field generated by an electric current that is constant. And the third law predicts how a magnetic field will interact with an electrical circuit to create an electromotive force. These laws were succeeded by the equations of J. C. Maxwell, presented in 1864, that characterize how the magnetic and electric fields are created and changed by one another (Lu et al., 2016).

Then in 1873, Maxwell published a book with the title *A Treatise on Electricity and Magnetism* (Maxwell, 1873), that united the study of electrical energy and magnetism, and from that moment magnetism and electrical energy were acknowledged to be regulated by the same force (Lu et al., 2016).

In 1884, J. H. Poynting perceived that the Poynting vector, which represents the directional density of energy flow from an electromagnetic field, would be essential in the quantification of electromagnetic energy. Then, in 1888, H. Hertz was the first one who successfully managed to demonstrate experimental proof of radio waves through his transmitter radio with spark-gap (Singh et al., 2012).

Several steps marked the history of Wireless Power Transfer. In the 1920s and 1930s, magnetrons were invented to convert electrical energy into microwaves, which allowed the transmission of power wirelessly over long distances. On the other hand, there wasn't a method at the time to convert microwaves back to electrical energy. For that reason, the development of charging without wires was left behind (Lu et al., 2016).

In 1961, W. C. Brown published the first article suggesting the use of microwave

energy for the transfer of power. Then in 1964 he exhibited a model of an helicopter that was charged by microwaves, i.e. a vehicle that rides on a microwave beam and takes from the beam all the necessary energy for its propulsion (Brown et al., 1965). This helicopter then inspired the research that followed of airplanes powered by microwaves during the 1980s and 1990s in Canada and Japan (Schlesak et al., 1988).

Also in 1964, Brown performed the transformation of microwaves to electrical energy through a rectifying antenna, that directly converted microwaves into direct current (Singh et al., 2012). In 1975, he transmitted 30 kW of power through 1,6 km with an effiency of 84% in the Venus Site of the NASA's Jet Propulsion Laboratory (JPL) in the Goldstone Deep Space Communications Complex (GDSCC), also known as Golstone Observatory (Strassner & Chang, 2013).

In 1968, the idea of putting a large Solar Power Satellite (SPS) in the geostationary orbit of the planet to gather energy from the light of the sun and then transmit that energy back to the planet through an electromagnetic beam was introduced. During the 1970s and 1980s, NASA had a project on SPS that allowed for major developments in large-scale microwave transfer of energy. At the same time, the technology based on coupling was slowly developed (Lu et al., 2016).

In 1975, there were experiments of power transfer without the use of cables in the span of dozens of kilowatts at the Goldstone Observatory (Brown, 1984). Then in 1987, it was reported that an airplane free of fuel was powered by the energy of microwaves, which was called Stationary High-Altitude Relay Platform (SHARP) (Schlesak et al., 1988).

In 2003, NASA's Dryden Flight Research Center demonstrated an airplane indoors powered by laser and in 2004 Japan suggested the charge without wires of an electrical motor by Microwave Power Transmission (Mohammed et al., 2010).

In the 2007 Consumer Electronics Show, a company named Powercast introduced Radio Frequency (RF) energy in the technology of WPT. On the same year, a research group of physics led by Professor Marin Soljačić at the Massachusetts Institute of Technology (MIT) showed the wireless powering of a 60 W light bulb with an efficiency of 40% and a 2 m distance using two coils with a radius of 30 cm, in a system that they called "WiTricity". Then in 2008, Intel recreated the experiment of MIT by powering a light bulb without wires at a lower distance with 75% efficiency (Mohammed et al., 2010).

Thanks to the MIT research there is a resurgence of interest and research effort in contactless energy transfer systems since it was proven to be possible to transfer energy wirelessly over long distances.

Wireless Power Transfer can be divided into two techniques defined by the physical phenomena of electromagnetic field propagation, that changes the distance at which the receiving and transmitting coils are: near-field (non-radiative) and far-field (radiative).

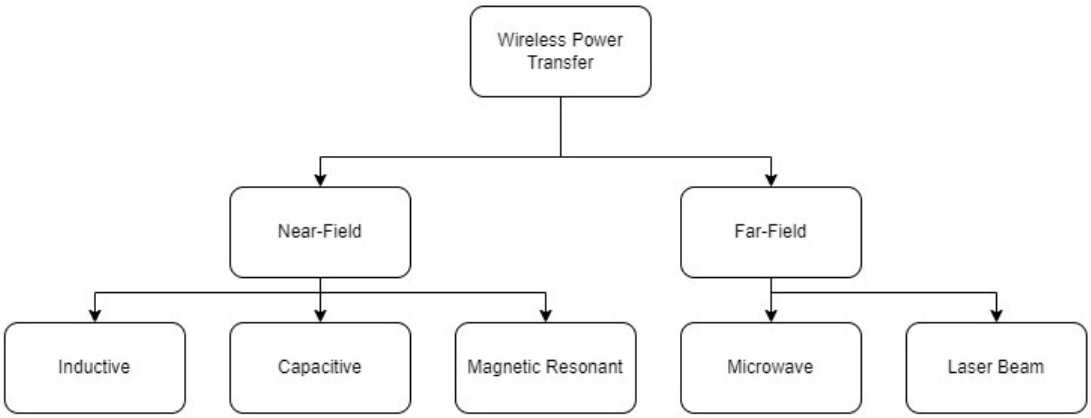

Figure 2.3: Techniques of Wireless Power Transfer.

2.1.2 Near-Field Techniques

Near-field techniques involve the application of a magnetic field and the use of inductive methods to transport energy across relatively smaller distances, typically up to several centimeters. Within these techniques, three methods can be distinguished: inductive coupling, capacitive coupling, and magnetic resonance coupling.

Inductive Technique (Inductive Coupling)

This method is based on the principle of magnetic field induction that transports electrical energy amid two coils.

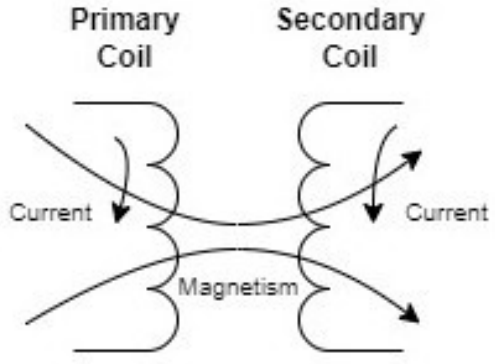

Figure 2.4: Schematic of the Inductive Coupling Technique (Lu et al., 2015).

It is explained by the laws of Biot-Savart and Faraday (Mou & Sun, 2015). The first one is used to calculate the value of the magnetic field originated by the current distribution:

$$B = \frac{\mu_0}{4 \cdot \pi} \oint \frac{I \cdot d_I \cdot r}{|r|^3}, \tag{2.1}$$

where μ_0 is the magnetic permeability of the air, I is the current that passes through the transmitter coil, d_I is a vector with a magnitude equal to the length of the differential element of wire, and r is the full displacement vector from the wire element to the point at which the field is being determined.

The second one is used to determine the value of the induced voltage over the receiver coil as the magnetic field varies along a surface:

$$V_{Ind} = -\frac{\partial}{\partial t} \oint B \cdot d_s. \tag{2.2}$$

The use of these laws means that when the primary coil of a transformer produces a magnetic field across the secondary coil, it induces a voltage over it.

The energy efficiency of this system depends on the tightness of coupling and the quality factor of the coils. The first one is based on the alignment, distance, and shape of the coils. The quality factor of the coils depends mostly on the materials that constitute them, considering its the size and shape as well as the frequency at which they operate (Lu et al., 2015).

This system has several advantages, of which can be highlighted its security since there are no exposed conductors which reduce the risk of electric shock; reliability; low maintenance; long product life; and waterproofing, because all the connections are closed (Faruk et al., 2017; Khutwad & Gaur, 2016).

The main applications of this technique are electric toothbrushes, charging pads for cell phones and laptops (Khang et al., 2018), such as the ones used by Samsung, LG, Sony, Nokia, Google, and Huawei (Kinsky, 2021).

This is the most used technique of WPT and will be the one used further in this dissertation.

Electrostatic Inductive Technique (Capacitive Coupling)

This method is used for low-power applications. The energy is transferred between metallic plates by the oscillation of an electric field with high frequency. On the side of the receiver, a battery is supplied by the capacitive current that is transported. When it comes to efficiency this system is restricted by the distance between the transmitter and receiver plates (Valtchev et al., 2012).

It has some advantages when compared to inductive coupling. By using capacitors the system becomes much simpler and with a lower cost and electromagnetic radiation. It also has the advantage of not needing components of magnetic flux guidance and shielding. On the other hand, the capacitance's amount of coupling depends on the area of the device that is available and the increase of the size of the capacitors, to increase the area, may not be ideal in some applications (Faruk et al., 2017).

However, the main advantage of capacitive coupling is that an electric field can penetrate through a metal shielding and due to this it can't just transmit through metal

but also has a nice ability of anti-interference of the magnetic field (Yusop et al., 2016).

Electrodynamic Inductive Technique (Magnetic Resonant Coupling)

This method is based on the magnetic resonance principle, which means that at a specific frequency, the reactances of the transmitting and receiving coils are equal to one another. This happens when the primary coil, loaded with capacitors, oscillates to create a magnetic field (Barman et al., 2015; Thakur & Abrol, 2017). This system can be characterized by an RLC circuit.

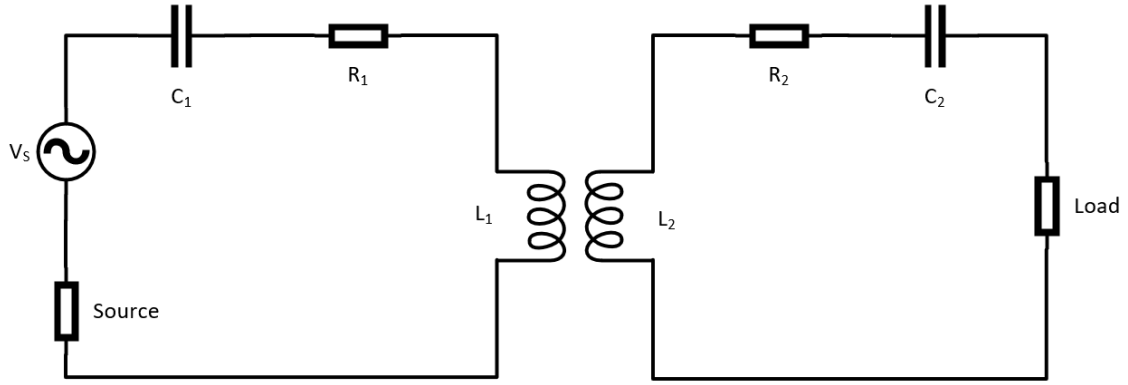

Figure 2.5: The equivalent WPT circuit based on Magnetic Resonant Coupling (Mou & Sun, 2015).

Its efficiency depends on the coupling coefficient between the coils and their quality factor. The bigger both factors are, the bigger is the efficiency. A high quality factor means that there is a small loss rate in the exchange of energy in the coils, while a high coupling coefficient means a higher coupling rate (Wang et al., 2013).

When compared to the inductive coupling method, the magnetic resonant one has the advantage of functioning even if the coupling coefficient between the coils is low, i.e. smaller than 0,2, unlike the coupling coefficient of the inductive coupling technique that needs to be close to 1 (Wang et al., 2013).

Some of this technique's applications are the charging of implantable devices, electric vehicles and Wireless Sensor Networks (WSN) (Khang et al., 2018).

2.1.3 Far-Field Techniques

Far-field techniques involve the transmission and reception of radiated electromagnetic waves to transport energy across larger distances, in the range of several meters. Inside these techniques, there can be distinguished two methods: microwave radiation and laser beam.

Microwave Technique

This technique uses a directed microwave beam that sends energy from the transmitter to the receiver. It needs a correct alignment and no obstacles in its line of sight because otherwise there is no transfer of energy to the receiver coil (Wang et al., 2013).

This technique's main disadvantage is that the significant part of the radiating energy does not reach the given area of space because of the diffraction divergence, i.e. as the transmission distance increases as compared to the diffraction length of the radiating antenna (Shaposhnikov, 2002).

However, there are possible applications for this technique. A stationary high altitude relay platform can be used to power an aerial vehicle free of fuel from the ground to the Stratosphere, or in a space solar power satellite placed in the geostationary orbit, which would be able to transmit the power that was created in the satellite via microwave to a fixed region on the planet (Hu et al., 2021).

Laser Beam Technique

This technique consists of the transmission of power under visible or near-infrared frequency. To achieve an efficient transfer of energy over long distances, it uses a laser beam that is highly concentrated directed at the receiver (Sidiku et al., 2021).

It has the advantage of the energy being concentrated into one single point. Nevertheless, the radiation from the laser can be very harmful and it is very difficult to have the laser pointing accurately to the receiver. And when compared to the microwave technique, the laser beam is more vulnerable to the absorption of the atmosphere and the weather itself (Sidiku et al., 2021).

2.1.4 Compensation Topologies

A system with two coils is weakly coupled with leakage inductances, which makes necessary the use of compensation topologies. Figure 2.6 shows the most common topologies used in non-contact power transfer systems.

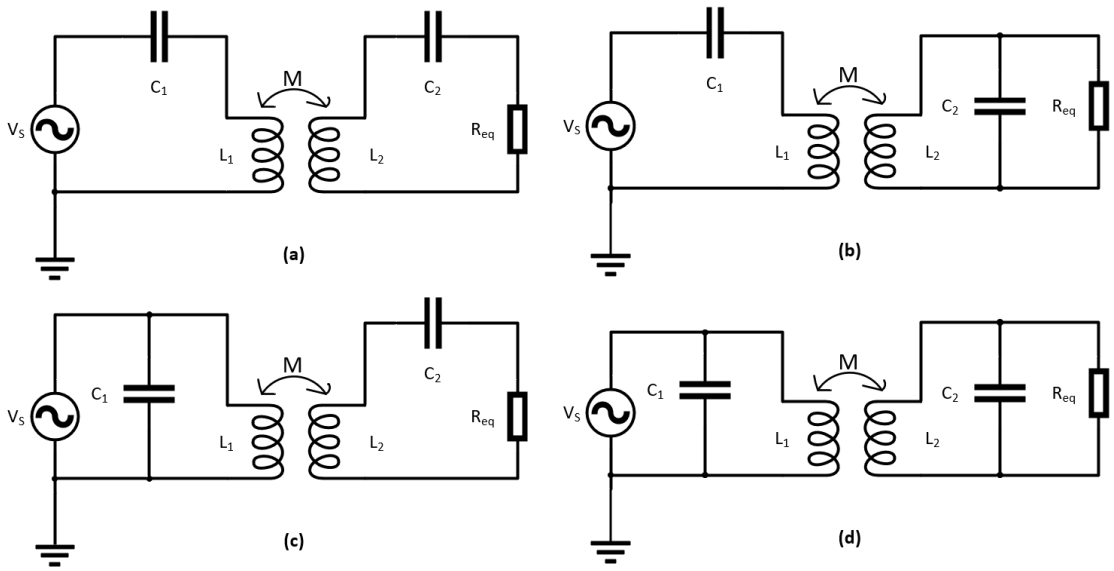

Figure 2.6: Compensation Topologies: (a) Series-Series, (b) Series-Parallel, (c) Parallel-Series, and (d) Parallel-Parallel (Bi et al., 2016).

On the transmitter side, the topology is used in a way that there is a minimization of the apparent power, through the null phase angle, so that there it's not necessary for the power supply to provide reactive power. On the receiver side, the compensation has the function of adjusting the circuit so that it is in resonance with the transmitter circuit to exist a maximization of the transfer power (Bi et al., 2016).

The nomenclature used to describe the topologies concerns the positioning adopted for the capacitors in relation to the coils, as indicated in Table 2.1.

Table 2.1: Characterization of the compensation topologies (Kalwar et al., 2015).

Topology	Acts as	Total impedance at resonant state	Efficiency
Series-Series	Voltage source	Low	Very high
Series-Parallel	Current source	Low	Medium
Parallel-Series	Voltage source	High	Medium
Parallel-Parallel	Current Source	High	High

Comparing the presented compensation topologies, Series-Series and Series-Parallel are the best adequate, economically, for high power transfer. Regarding the Parallel-Series and Parallel-Parallel topologies, the load variations influence the capacitance of the receiver circuit, while in the other two topologies that doesn't happen, making this the most suitable for load conditions that vary since the resonance is guaranteed (Bi et al., 2016).

2.2 Superconductivity

2.2.1 Introduction and History Perspective

The history of Superconductivity begins in the year 1911 when Dutch physicist H. Kamerlingh Onnes discovered that below the temperature of 4.2 K (-268,95 °C) the resistivity of mercury was null. After that, he discovered that when a magnetic field was applied it lowered the critical temperature of the material, i.e. the temperature at which the material presented a virtually null resistance. If that field is sufficiently intense, the superconductivity disappears and the material changes from the superconductor state to its normal state (Roque et al., 2017).

In the year of 1933, Walter Meissner and Robert Ochsenfeld discovered that superconductors are perfect diamagnets, i.e. they repel the magnetic flux within them. This phenomenon became acknowledged as the Meissner effect (Mourachkine, 2004).

Then in 1935, German brothers Friz and Heinz London proposed a theory to describe the macroscopic phenomenons of the superconductor state. This theory encompasses two equations that describe the electric and magnetic fields in superconductors (Mourachkine, 2004).

In 1957, J. Bardeen, L. Cooper, and R. Schrieffer elaborated the first microscopic theory of superconductivity, which allows to explain many of the phenomena of the superconductors discovered until then. It introduces the so-called pairs of Cooper, which are associations of pairs of electrons that work as charge carriers in superconductors. This theory is known as the BCS theory (Mourachkine, 2004).

In the same year, Alexei Alexeyevich Abrikosov theoretically predicted the existence of a new kind of superconductors, that he called type II superconductors to distinguish from the already existent type I. With this, Abrikosov introduced the mixed state, in which the normal and superconducting phases coexist in the material (Tinkham, 2004).

The interest in applications based on superconducting materials gained a new impulse when J. Georg Bednorz and K. Alexander Müller discovered high-temperature superconductivity. The critical temperature that they found was first higher than 77,3 K (-195,85 °C), which is the boiling point for liquid nitrogen under normal conditions of pressure, and then higher than 100 K (-173,15 °C). This allowed the possibility of substituting liquid helium, a very costly and nonrenewable coolant used until then, for liquid nitrogen, a much cheaper coolant (Chernoplekov, 2002).

2.2.2 High-Temperature Superconductors

The High-Temperature Superconductors (HTS) appear in two forms, or bulk or tape. To produce high-critical temperature superconductor coils, superconducting tapes are used. There are two types of superconducting tapes: first-generation tapes (1G) and second-generation tapes (2G).

First-Generation Tapes

The first developed tape superconductors, also known as first-generation tapes, are made up filaments of BSCCO (Bismuth-Strontium-Calcium-Copper-Oxide) superconducting materials, that are immersed in a silver matrix that make the tape more flexible and stronger mechanically. Commercially, there are two phases of these tapes, Bi-2212 and Bi-2223, having critical temperatures of 90 K (-183,15 °C) and 110 K (-163,15 °C), respectively (MA, 2004).

Second-Generation Tapes

Second-generation tapes, also known as YBCO (Yttrium-Barium-Copper-Oxide) coated conductors, are tapes made of thin films deposited on substrates. They have higher fields, temperatures and critical current densities than the ones found in the 1G tapes. For that, they are more expensive than the 1G tapes (MA, 2004).

For the present dissertation planar superconducting coils will be used, using second-generation superconducting tape, due to its better mechanical properties.

2.3 Wireless Power Transfer with Conventional Coils *Versus* Superconducting Coils

In the previous section, it was explained how superconductivity works and what are the advantages of using it. In the last few years, there has been a great deal of research on how to enhance the efficiency of WPT systems, because copper coils have a current carrying capacity that is limited and a quality factor which is low.

The quality factor of a coil is given by

$$Q = \frac{2 \cdot \pi \cdot f \cdot L}{R}, \tag{2.3}$$

where R is the value of the coil's resistance, L its inductance and f the frequency. Which means that in order for a coil to have a high-quality factor, its resistance and inductance need to be high and low, respectively (Jeong et al., 2017).

As mentioned before, high-temperature superconductors can transport electrical current with a virtually zero DC resistance, i.e. they can have a high quality-factor, and have a transition temperature above 77 K (-196,15 ºC), which allows the use of liquid nitrogen for cooling. These two characteristics make them the most suitable to be applied in WPT systems to increase their efficiency. They can even compensate for a weak coupling configuration due to their high current carrying capacity and close to zero power losses (Utschick, 2021).

However, there are only zero losses in superconductors when they are in DC conditions. In AC, a part of the transmitted power is dissipated in the superconductor. Although these

losses are small and may not influence the efficiency of the system, they increase the temperature of the superconductor. If the temperature of the superconductor becomes greater than its critical temperature then the material will no longer be in the superconducting state. And because AC losses increase with the increase of the current and frequency there can be a problem when working with these coils in a WPT system. To solve this problem, cooling modules can be used to lower the temperature of the coils below its critical one, making their sustained operation possible in the superconducting state (Machura et al., 2020; Utschick, 2021).

2.4 Power Supply

AC/DC converters are the most common power supplies (as well as DC/DC converters) and can be divided into linear and switched power supplies (Amaral & Cardoso, 2016). As a linear AC/DC converter will be the one used further in this dissertation, it will be the converter discussed in this section.

A linear power supply consists of a transformer, rectifier, filter and regulator, as depicted in Figure 2.7.

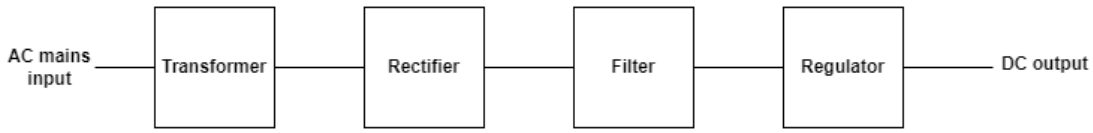

Figure 2.7: Schematic of a power supply (Jones, 2012).

The transformer is used to ensure that there is electrical isolation between the AC source and the power supply output. Then, the rectifier transforms the AC voltage from the transformer to a DC one. After the rectification there's a voltage ripple that the filter decreases and, also, increases the mean output voltage. Lastly, the regulator converts the output DC voltage of the filter from unregulated to regulated (Amaral & Cardoso, 2016).

2.4.1 Rectification

A full-wave rectification circuit can be implemented with two or four diodes. The circuits with four diodes are called bridge circuits and have the same output voltage as the ones with two diodes, but the circuit is closed with two diodes instead of one. The use of these types of circuits allows for a simpler power source because there it's not necessary the use of a bipolar power supply. However, the load is linked to the source by two diodes in series, that reduces the efficiency of the rectifier because there's an increase in the loss of voltage at the p-n junctions of the diodes. Due to this, bridge circuits are used when working with small load currents and a larger rectified voltage than the one of the open p-n junction, as happens in this dissertation (Solovyeva et al., 2021).

Figure 2.8 presents the schematic of a full-wave bridge rectifier, while Figure 2.9 shows its output voltage.

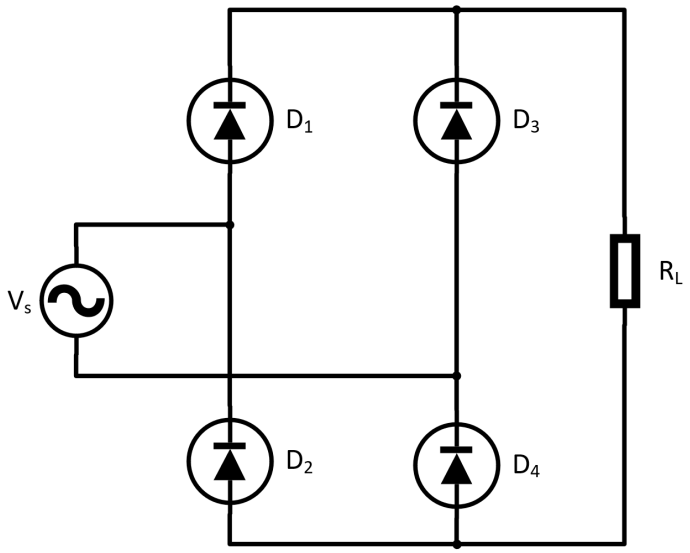

Figure 2.8: Schematic of a full-wave bridge rectifier.

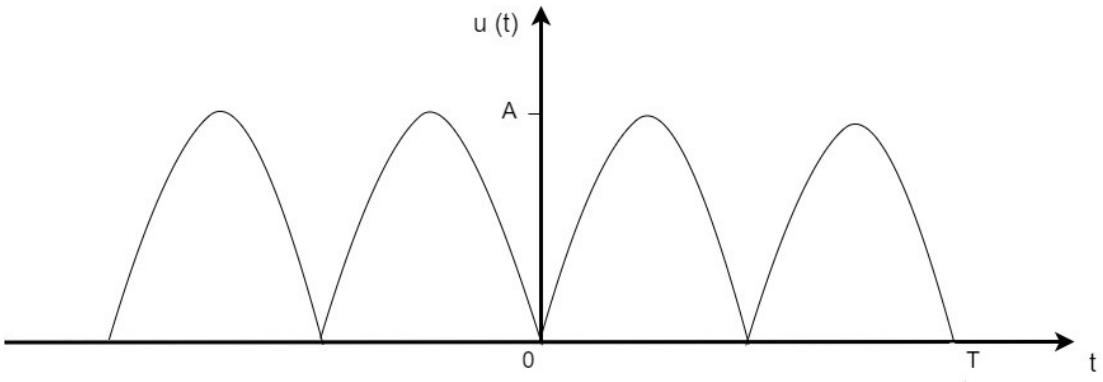

Figure 2.9: Output voltage of an ideal full-wave bridge rectifier (Solovyeva et al., 2021).

2.4.2 Filtering

To allow the passage of the load's DC component and block the AC one of the rectifier's output a filter is used. For this, capacitors and coils are chosen because capacitors smooth the voltage, while coils smooth the current. To allow the passing of the DC component but limit the passage of high-frequencies a low-pass filter is used. The simplest form of this type of filter is a capacitor in parallel with the load resistor (Plonus, 2020).

Figure 2.10 shows the schematic of a full-wave bridge rectifier with an RC filter.

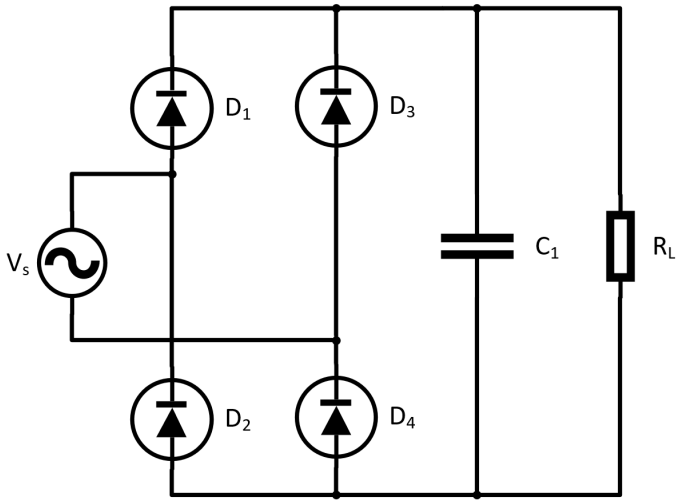

Figure 2.10: Schematic of the rectifier with an RC filter.

Ripple

During discharging, the voltage of the capacitor decreases. It starts equal to V_p and when t = t_2 its equal to

$$v_o = V_p \cdot e^{\frac{-(t_2-t_1)}{R_L \cdot C}}. \tag{2.4}$$

The time of discharge is on the order of the period T of the input voltage, which means that t_2 - t_1 can be approximated by T, i.e. t_2 - $t_1 \approx$ T. The voltage ripple v_r is then given by,

$$v_r = \Delta v_o = V_p - V_p \cdot e^{\frac{-T}{R_L \cdot C}} \approx V_p \cdot \frac{T}{R_L \cdot C} = \frac{V_p}{f \cdot R_L \cdot C}, \tag{2.5}$$

where it's assumed that $\frac{T}{R_L C} \ll 1$, which guarantees a small decrease during the discharge and due to that a small voltage ripple (Plonus, 2020). In equation (2.5) the last term means that the voltage ripple is inversely proportional to the filter's capacitance, i.e. the higher the capacitance the smoothest the DC component (Plonus, 2020).

2.4.3 Regulation

In order to maintain a fixed output voltage of the system despite changes in input voltage or the variation of the load's conditions, a voltage regulator is used. It can be used for DC/DC, AC/AC or AC/DC power conversion.

There are two types of voltage regulators: linear or switching. The first one uses an active pass device, controlled by a high gain operational amplifier. To keep the output voltage constant, the linear regulator compares the output voltage with a reference voltage, thereby adjusting the resistance value of the active device. A switching regulator converts the input voltage to a switched one applied to a power MOSFET or BJT switch. The filtered power switch output voltage is fed back to a circuit that controls the power switch on and

off times so that the output voltage remains constant regardless of input voltage or load current changes (Osanlo et al., 2020).

Linear regulators are step-down converters, which means that their output voltage is always lower than their input voltage. However, they have the advantages of offering low noise and low voltage ripple when compared to the switching ones (Osanlo et al., 2020). This is why a linear voltage regulator will be further used in the present dissertation.

Figure 2.11 shows the schematic of a linear voltage AC/DC converter.

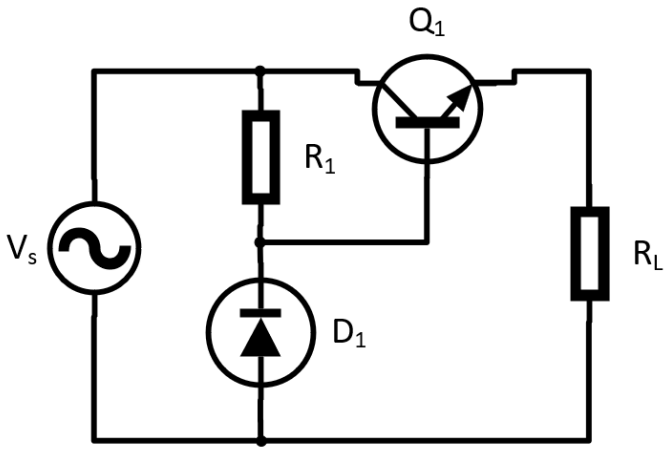

Figure 2.11: Schematic of a linear voltage AC/DC converter.

2.5 Chapter Summary

This chapter presented the main scientific works developed in the area of WPT, namely the different techniques that exist and the compensation topologies that can be used. A bibliographic survey was also carried out in order to understand how superconductivity works, specifically referring to high-temperature superconductors and how they can contribute to the improvement of contactless energy transfer systems.

Finally, the various components of a power supply system were referenced in order to understand how they work and, thus, be able to correctly know how the charging of a battery needs to be done.

In the next chapter, the methodology performed in this dissertation is presented. First, the equations that compose a voltage controlled battery and then the ones that are necessary for the implementation of a wireless power transfer system.

3

Methodology

This chapter presents the methodology adopted (Figure 3.1) as well as the concepts necessary for the design of a contactless power transfer system for charging a lead acid battery.

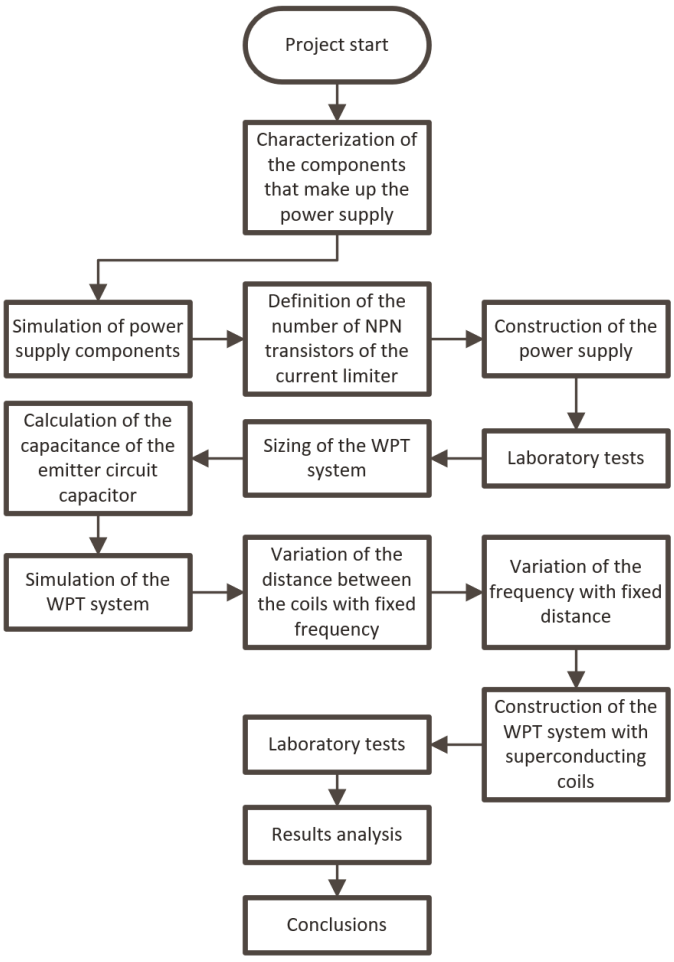

Figure 3.1: Flowchart of the methodology applied in the sizing of the WPT system with power supply.

3.1 Battery

To be able to test the behaviour of a battery with injected voltage, a controlled voltage source in series with a constant value resistance can be used as presented in Figure 3.2 (Tremblay et al., 2007).

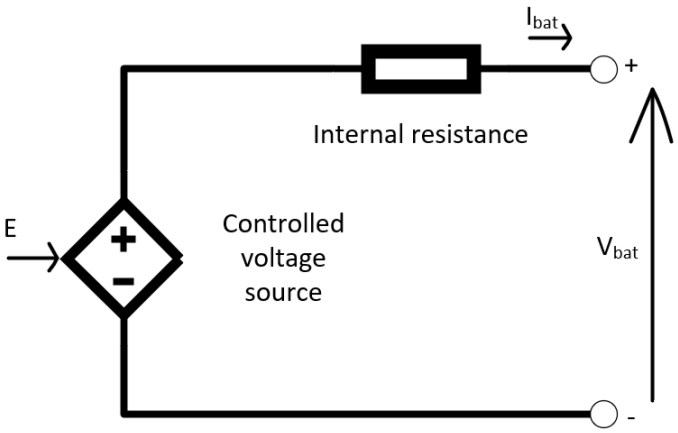

Figure 3.2: Circuit diagram of a constant voltage battery (Tremblay et al., 2007).

The open circuit voltage source can be calculated using a non-linear equation based on the SoC of the battery, described by

$$E = E_0 - K \cdot \frac{Q}{Q - i \cdot t} + A \cdot e^{-B \cdot i \cdot t}, \tag{3.1}$$

where E is the sampling signal, E_0 is the constant voltage, K is the polarisation voltage, Q is the battery capacity, A is the battery exponential, B is the inverse exponential of the capacity in function of time, i is the current of the circuit, and t is the time.

The voltage of the battery V_{bat} is given by

$$V_{bat} = E - R \cdot i, \tag{3.2}$$

where R is the internal resistance of the battery.

This model is based on specific assumptions:

- The internal resistance is considered constant during the load cycle and does not vary with the value of the current.
- Battery capacity does not change with current amplitude (no Peukert effect[1]).
- Temperature does not affect the behaviour of the model.

[1]The Peukert effect is the change in the capacity of a rechargeable lead-acid battery at different rates of discharge, expressed by Peukert's law.

But has some limitations:

- The minimum no-load battery voltage is 0 V and the maximum battery voltage is not limited.
- The minimum battery capacity is 0 Ah, but the maximum capacity is not limited, contrary to what happens with the model used for the simulation with a constant current. As there is no limitation, the maximum SoC can be greater than 100% if the battery is overloaded.

3.2 Inductive Power Transfer

The inductive coupling method, also named inductive power transfer, is based on the principle of magnetic field induction that transports electrical energy between two coils. Figure 3.3 depicts its equivalent circuit, where L_1 and L_2 are the self-inductances of the emitter and receiver circuit, respectively. k_{12} is the coupling factor between the two coils. R_s and R_L are the source and the load resistances, respectively. R_{p1} represents the resistance in the transmitting loop.

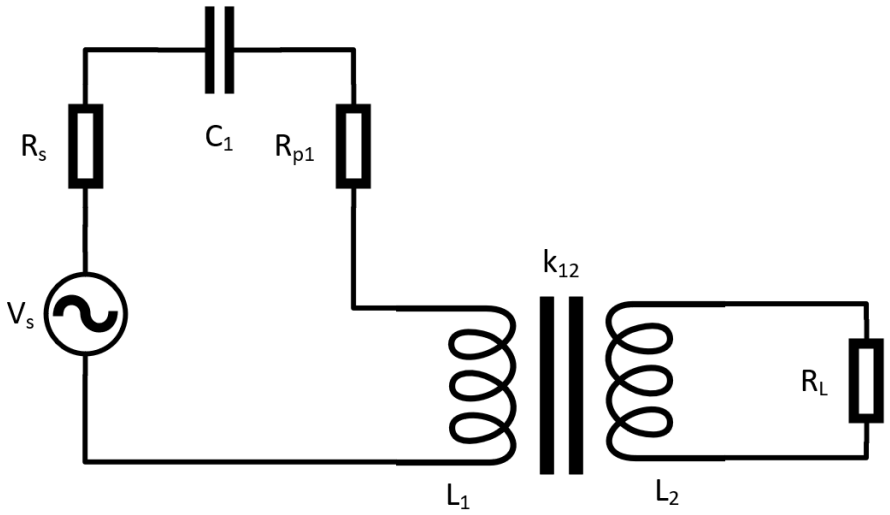

Figure 3.3: Equivalent circuit of the Inductive Coupling Method.

The coupling factor k_{12} is given by

$$k_{12} = \frac{M_{12}}{\sqrt{L_1 \cdot L_2}}, \tag{3.3}$$

where M_{12} is the mutual inductance of the two coils, L_1 is the self-induction of the emitter coil and L_2 is the self-induction of the receiver coil.

k_{12} can have values between 0 and 1. If $k_{12} = 0$, then there is no magnetic coupling between the two coils, which means that the flux created by the emitter coil doesn't reach the receiver one. When $k_{12} = 1$, the coupling is perfect because there is no dispersion flux (Waffenschmidt, 2011).

In order to calculate the mutual inductance of the two coils in the MATLAB/Simulink simulations, the following equation is used (Zouaoui et al., 2022)

$$M_{12} = (-L \cdot d) + 0,165, \tag{3.4}$$

where L is the value of the inductance of the coils, considered to be equal in both of them, and d is the distance between the coils in cm.

Experimentally the mutual inductance is obtained through (Budhia et al., 2013)

$$M_{12} = \frac{U_{OC}}{\omega \cdot I_1}, \tag{3.5}$$

where U_{OC} is the open circuit voltage of the receiver, I_1 is the current related to the emitter circuit and ω is the angular frequency.

The mathematical equations describing the channel of the system considering the equivalent circuit shown in Figure 3.3 are (Budhia et al., 2013)

$$\begin{cases} \left(R_{eq1} + j \cdot \omega \cdot L_1 + \frac{1}{j \cdot \omega \cdot C_1}\right) \cdot I_1 - j \cdot \omega \cdot M_{12} \cdot I_1 = V_s \\ (R_L + j \cdot \omega \cdot L_2) \cdot I_2 - j \cdot \omega \cdot M_{12} \cdot I_1 = 0 \end{cases} \tag{3.6}$$

where R_s is the source resistance, R_L is the load resistance, V_s is the source voltage, I_2 is the current related to the receiver circuit, and $R_{eq1} = R_s + R_{p1}$.

Considering $Z_1 = R_{eq1} + \mathrm{j} \cdot \omega \cdot L_1 + \frac{1}{j \cdot \omega \cdot C_1}$, $Z_2 = R_L + \mathrm{j} \cdot \omega \cdot L_2$, and applying the Kirchhoff Laws to the circuit comes that

$$I_1 = \frac{Z_2 \cdot V_s}{Z_1 \cdot Z_2 + \omega^2 \cdot M_{12}^2} \tag{3.7}$$

and

$$I_2 = \frac{j \cdot \omega \cdot M_{12} \cdot V_s}{Z_1 \cdot Z_2 + \omega^2 \cdot M_{12}^2}. \tag{3.8}$$

The general expression of the energy efficiency of a two-coil WPT system is given by (Osanlo et al., 2020; Plonus, 2020)

$$\eta = \frac{R_L \cdot I_2^2}{R_{eq1} \cdot I_1^2 + R_L \cdot I_2^2}. \tag{3.9}$$

Which can be simplified as

$$\eta = \frac{R_L \cdot M_{12}^2 \cdot \omega^2}{(R_L^2 + \omega \cdot L_2) \cdot (R_s + R_{p1}) + R_L \cdot M_{12}^2 \cdot \omega^2}. \tag{3.10}$$

For a circuit to be considered to be in resonance it's necessary that the inductive reactance and capacitance are equal, i.e. the resulting impedance has to be real. Which means that the value of the resonant frequency can be calculated by

$$f_r = \frac{1}{2 \cdot \pi \cdot \sqrt{L_1 \cdot C_1}}. \tag{3.11}$$

where C_1 is the electrical capacity of the emitter's capacitor.

3.3 Chapter Summary

This chapter presented the methodology used for the implementation of the power supply and the wireless power transfer systems. The equations necessary to calculate the coupling factor between the two coils that compose the WPT system, of the mutual inductance and the energy efficiency were presented.

In the next chapter, the implementation of this dissertation that was carried out will be presented. Starting with simulations performed in MATLAB/Simulink of the final part of the system, the power supply, and then the wireless power transfer. And finally the prototype created and the results obtained in the tests performed.

4

Implementation

This chapter begins with the presentation of the simulations carried out in MATLAB & Simulink (R2021a version) of the wireless power transfer system that was divided into two separate systems in order to understand them better. First, the power supply system, that is the output unit of the wireless power transfer system, and then the wireless power transfer without the power supply. After, the simulations performed of the complete system are presented.

At the end of the chapter, the constructed prototypes of the two components of the system are presented, as well as the results obtained experimentally.

4.1 Simulations

This section presents the simulations carried out in MATLAB with the help of the Simscape library in Simulink. In the first four subsections the operation of the various components of the power supply system are simulated individually. In the fifth section the simulation of the power supply system is presented, and in the last section the simulation of the behaviour of the wireless power system is presented.

4.1.1 Battery

First, it was simulated the charging by direct injection of the intended current of the battery model that exists in the Simscape library to see how this model works. Figure 4.1 shows the schematic of the circuit with a constant current of 20 A.

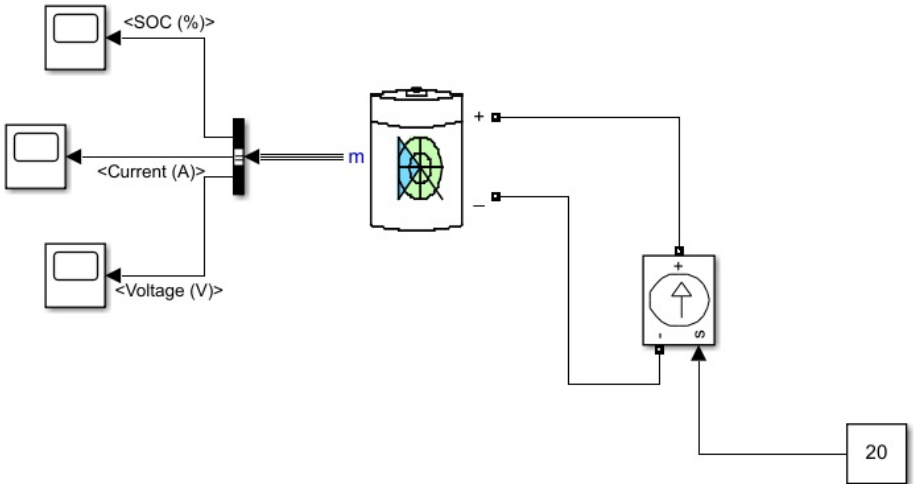

Figure 4.1: Electrical diagram of the developed simulation of the battery model with constant current, as implemented in MATLAB/Simulink.

This model of a battery allows to directly obtain the graphics of its State-of-Charge (SOC) and output voltage, as presented in Figures 4.2 and 4.3, respectively.

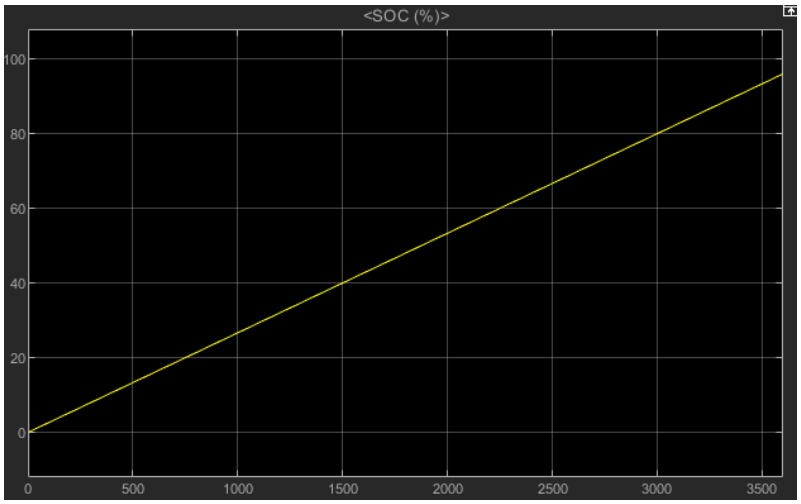

Figure 4.2: State-of-Charge behaviour of the constant current battery. Vertical axis is SoC (%), horizontal axis is time (s).

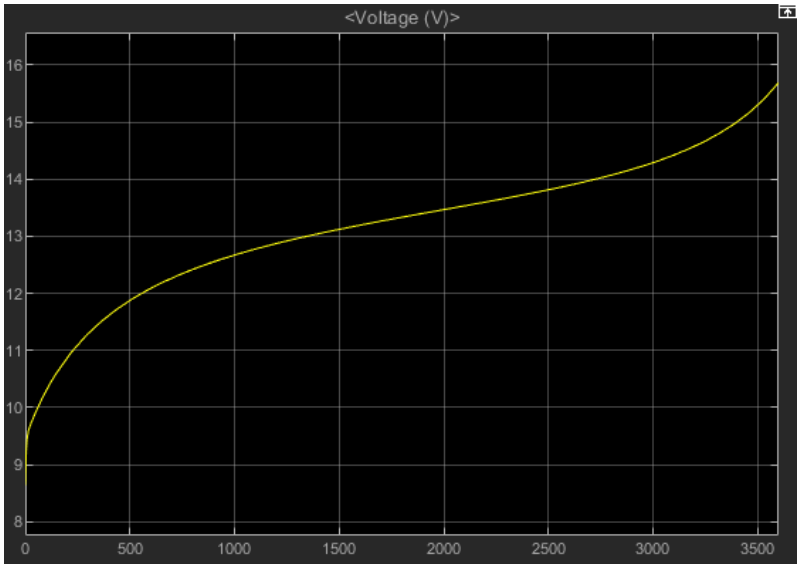

Figure 4.3: Voltage behaviour of the constant current battery. Vertical axis is voltage (V), horizontal axis is time (s).

After obtaining the graphics of the battery model with constant current, it was realised that to see the behaviour of a lead-acid battery with constant voltage injected, it needed to be used a different battery model.

The battery is now modelled using a simple controlled voltage source in series with a resistance of constant value, as was shown in Figure 3.2.

Table 4.1 shows the values of the parameters of the lead-acid battery's parameters.

Table 4.1: Lead-Acid battery parameters.

Parameter	**Value**
E_0 [V]	14
K [V]	0,4
A [V]	0,66
B $[(Ah)^{-1}]$	2884,6
R [Ω]	0,25
Q [Ah]	6,5

Having the values of the parameters, the model was simulated as depicted in Figure 4.4.

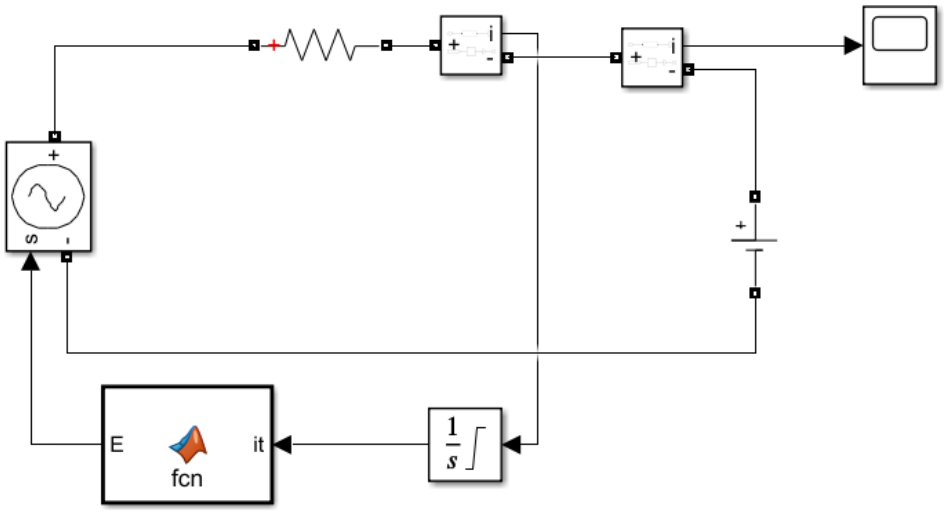

Figure 4.4: Electrical diagram of the developed simulation of the battery model with constant voltage, as implemented in MATLAB/Simulink.

As can be seen from Figure 4.4 a MATLAB function block was used where equation (3.1) was introduced with a integral block in order to integrate the current value obtained from the resistance, that simulates the internal resistance of a battery.

Figure 4.5 shows the obtained graphic of the current variation.

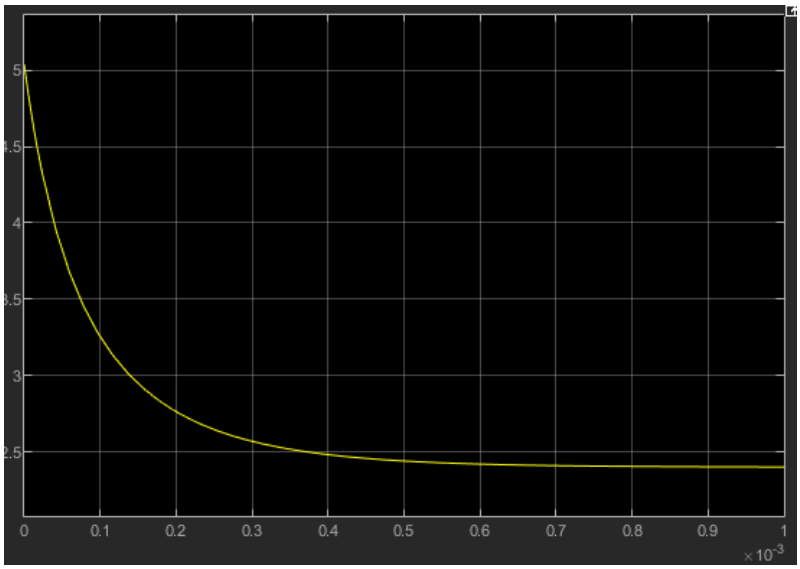

Figure 4.5: Current behaviour of the constant voltage battery. Vertical axis is current (A), horizontal axis is time (s).

After simulating the behaviour of a lead-acid battery it was considered that the power supply system of the battery is composed of a full-wave bridge rectifier, a filter and a voltage regulator.

4.1.2 Rectifier

In order to simulate the operation of a full-wave bridge rectifier, four diodes were used to make a bridge, in order to cancel the negative part of the wave coming from the transformer and project it to the positive part of the graph, by using the Simscape Library of Simulink. Thus obtaining the schematic shown in Figure 4.6, where the resistance is equal to 10 Ω.

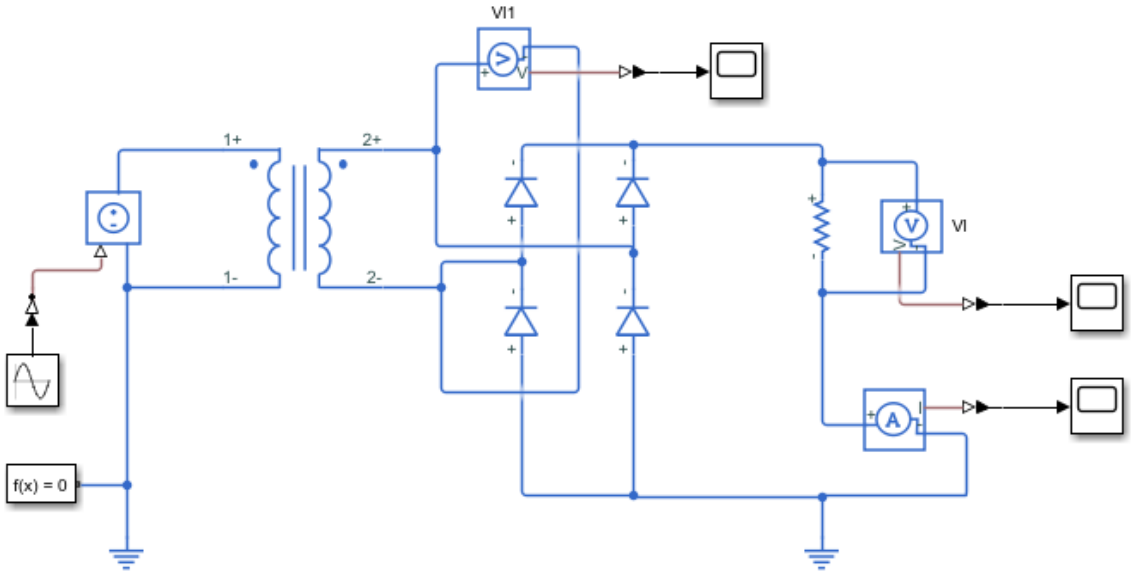

Figure 4.6: Electrical diagram of the developed simulation of the full-wave bridge rectifier, as implemented in MATLAB/Simulink with Simscape Library.

To verify the rectification of the wave coming from the transformer, voltage graphics were observed before and after the rectification, as presented in Figures 4.7 and 4.8, respectively.

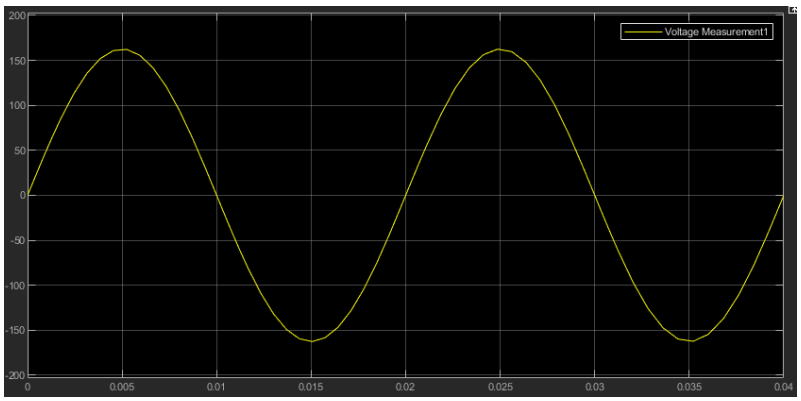

Figure 4.7: Voltage behaviour of the transformer. Vertical axis is voltage (V), horizontal axis is time (s).

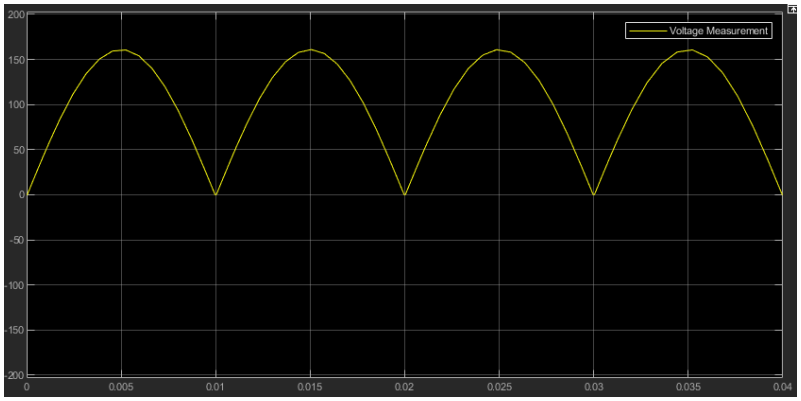

Figure 4.8: Voltage behaviour of the full-wave bridge rectifier. Vertical axis is voltage (V), horizontal axis is time (s).

In addition, the evolution of the current after the rectification was also observed as depicted in Figure 4.9.

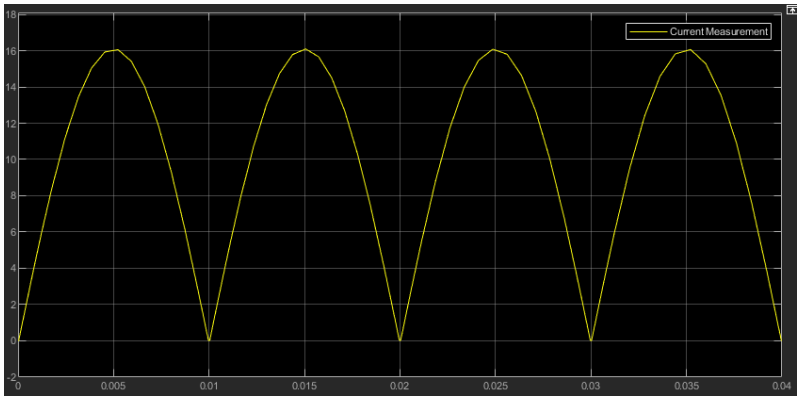

Figure 4.9: Current behaviour of the full-wave bridge rectifier. Vertical axis is current (A), horizontal axis is time (s).

4.1.3 Filter

To simulate filtering, first an RC filter was added to the schematic of Figure 4.6, resulting in the schematic of Figure 4.10. A capacitor of 4700 μF was used.

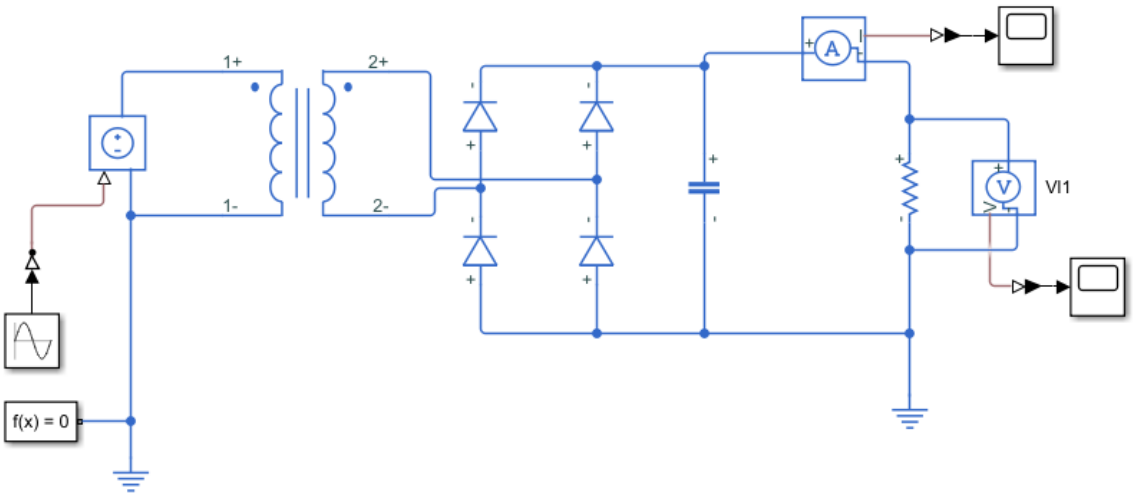

Figure 4.10: Electrical diagram of the developed simulation of the full-wave bridge rectifier with an RC filter, as implemented in MATLAB/Simulink with Simscape Library.

To see the effect of the filter on the output signal, circuit voltage and current graphics were observed, as presented in Figures 4.11 and 4.12, respectively.

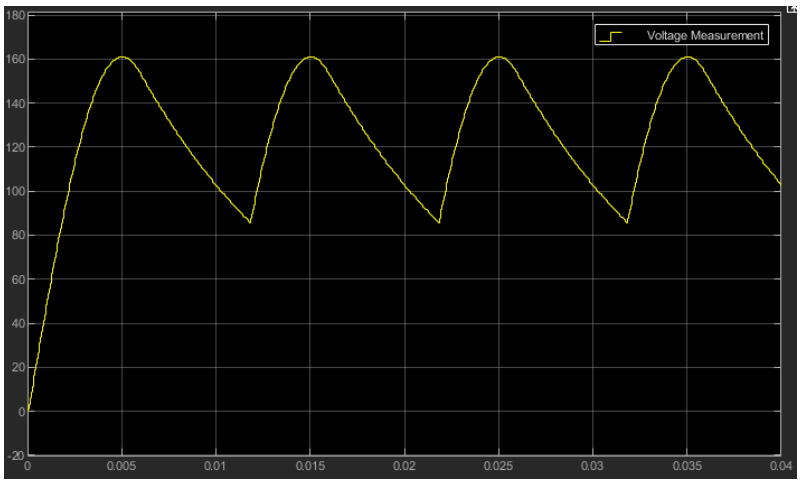

Figure 4.11: Voltage behaviour of the RC filter. Vertical axis is voltage (V), horizontal axis is time (s).

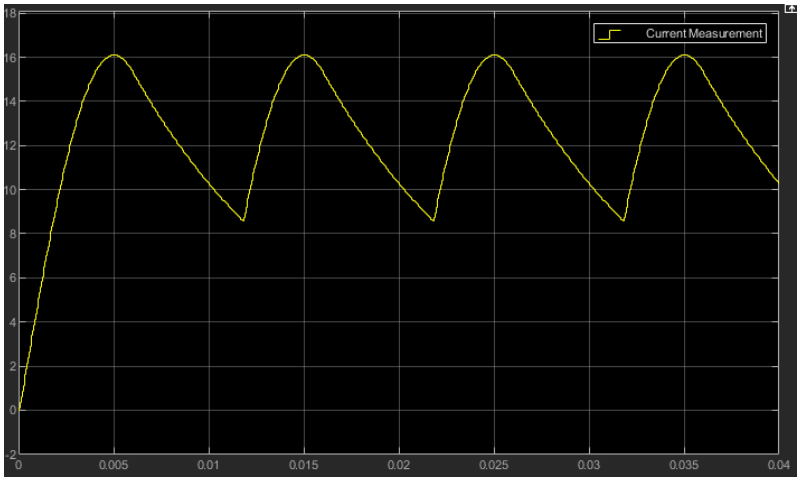

Figure 4.12: Current behaviour of the RC filter. Vertical axis is current (A), horizontal axis is time (s).

After simulating the RC filter the circuit was tested with a different filter. For example, a Pi filter, as depicted in Figure 4.13. As can be observed, this filter consists of an inductor with two capacitors in parallel, arranged like the Greek letter Pi. The input capacitor is selected to offer low reactance and repel the majority of the nuisance frequencies or bands to block. They present very-low impedances at high frequencies at both ends due to capacitive shunting. The inductor has an inductance value of 1,3 mH and both capacitors have a capacitance value of 4700 μF.

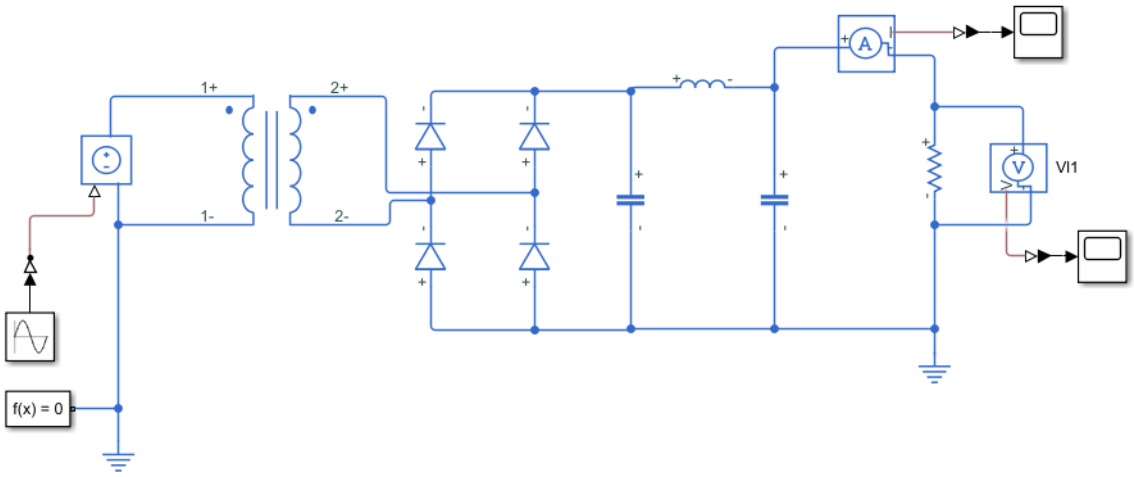

Figure 4.13: Electrical diagram of the developed simulation of the full-wave bridge rectifier with a Pi filter, as implemented in MATLAB/Simulink with Simscape Library.

The voltage and current output of the Pi filter were observed, and are presented in Figures 4.14 and 4.15, respectively.

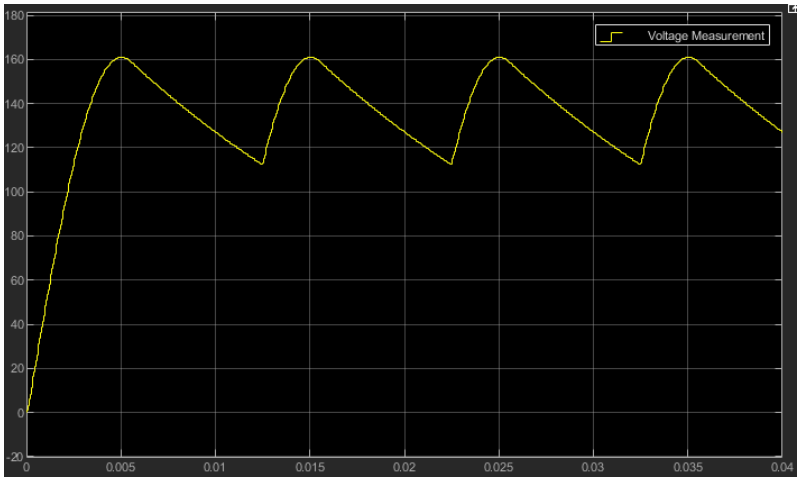

Figure 4.14: Voltage behaviour of the Pi filter. Vertical axis is voltage (V), horizontal axis is time (s).

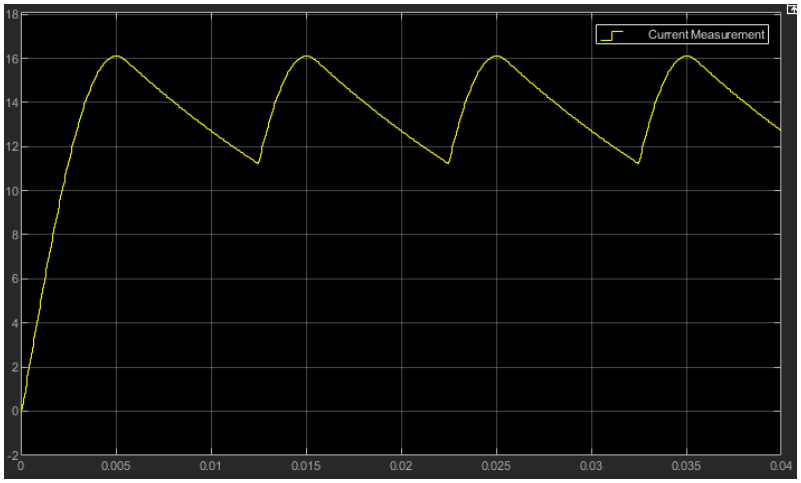

Figure 4.15: Current behaviour of the Pi filter. Vertical axis is current (A), horizontal axis is time (s).

4.1.4 Voltage Regulator

A voltage regulator consists of an active pass device, namely a diode. To keep the output voltage at a constant value, the regulator compares the output voltage with a reference one, thereby adjusting the resistance value of the diode. In Figure 4.16 the simulated regulator is presented.

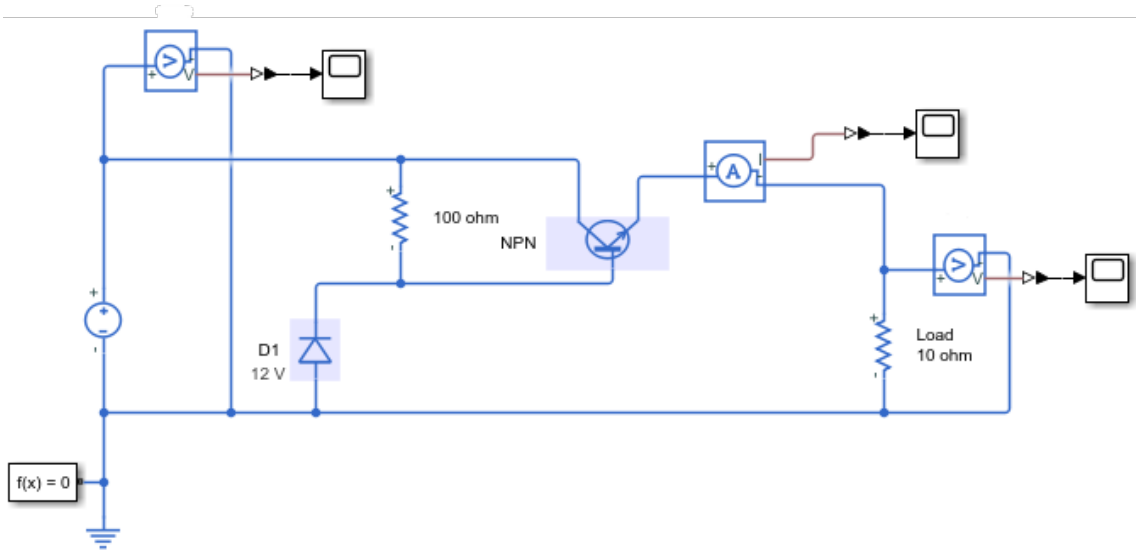

Figure 4.16: Electrical diagram of the developed simulation of the voltage regulator, as implemented in MATLAB/Simulink with Simscape Library.

For the voltage regulator to have a current limiter the number of NPN transistors in Figure 4.16, all connected in series, were increased from two to six and it was observed which was the optimal number. The behaviour of the output voltage and output current with the number of transistors varying are observed in Figures 4.17 and 4.18, respectively.

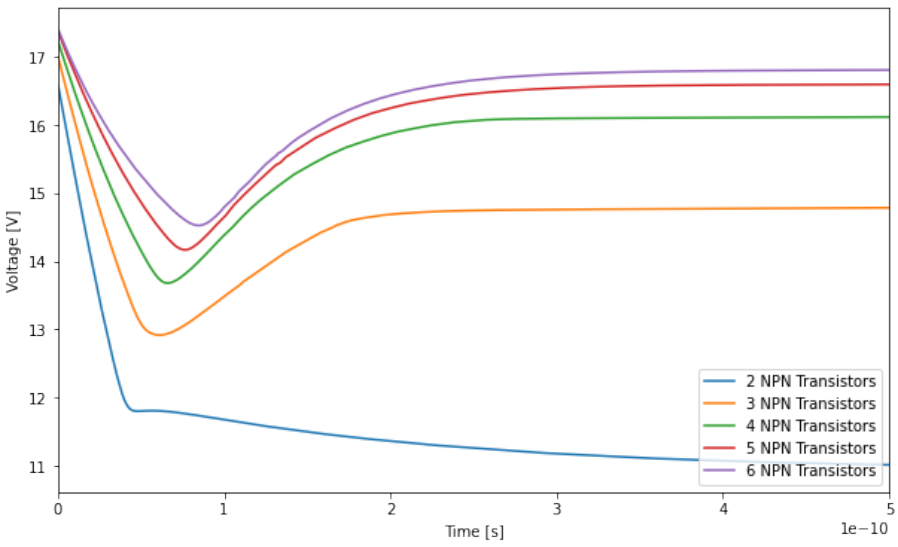

Figure 4.17: Voltage behaviour of a voltage regulator with variable number of bipolar transistors in series.

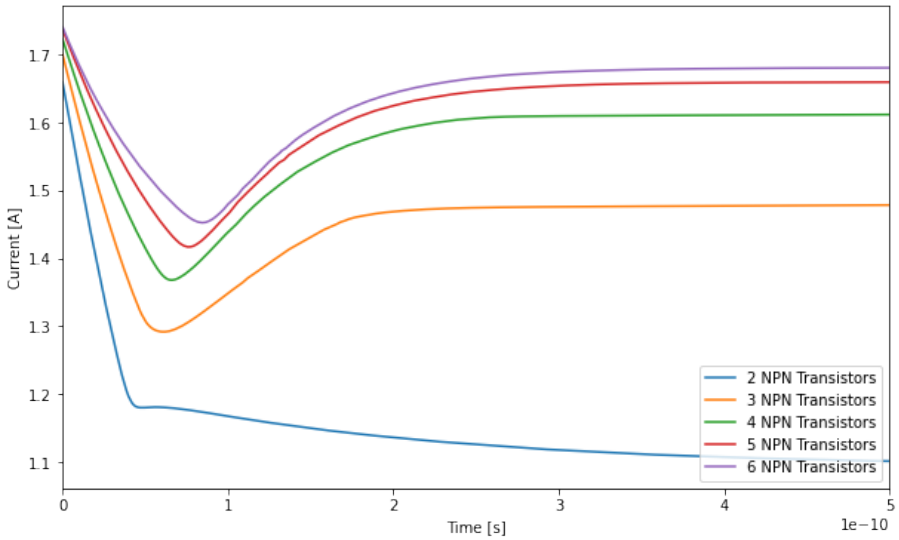

Figure 4.18: Current behaviour of a voltage regulator with variable number of bipolar transistors in series.

Since having five or six transistors connected in series the output voltage and current are very similar to having four and there is a considerable difference between having three and four transistors, it is chosen that the optimal value is four transistors, where it can be obtained a good constant current value.

4.1.5 Power Supply

In Figure 4.19 the power supply with the selected voltage regulator with four NPN transistors in series is presented.

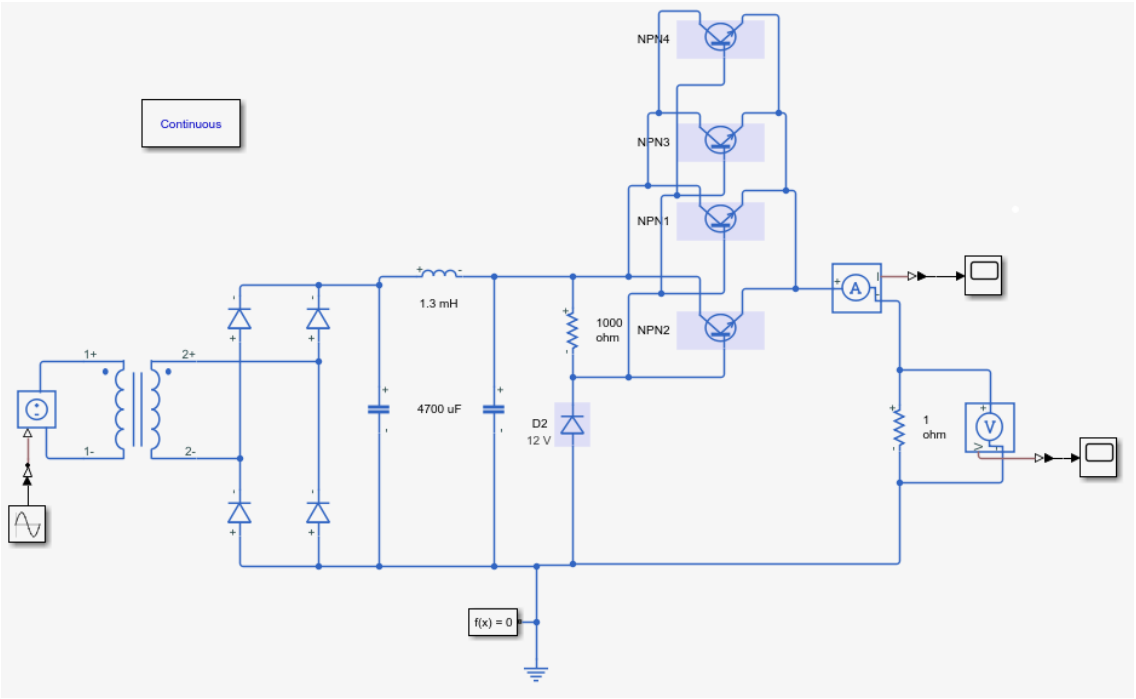

Figure 4.19: Electrical diagram of the developed simulation of the power supply, as implemented in MATLAB/Simulink with Simscape Library.

Figures 4.20 and 4.21 present the output voltage and current behaviours obtained from the schematic in Figure 4.19.

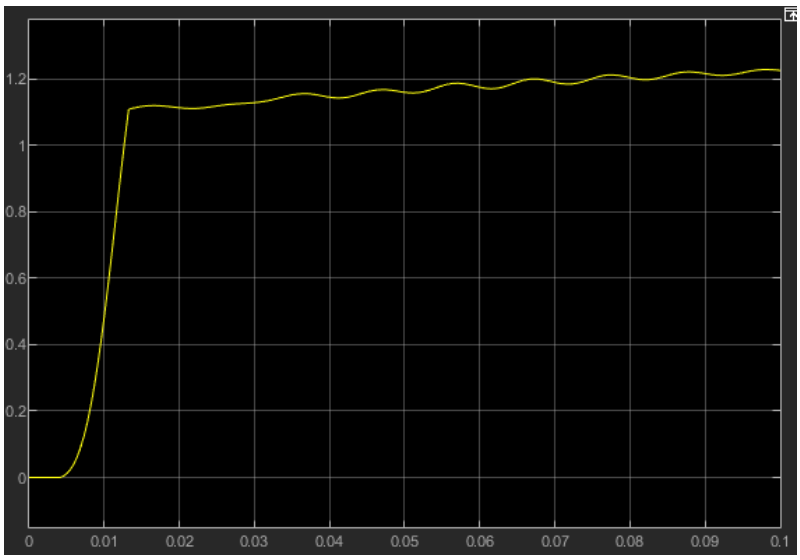

Figure 4.20: Current behaviour of the power supply. Vertical axis is current (A), horizontal axis is time (s).

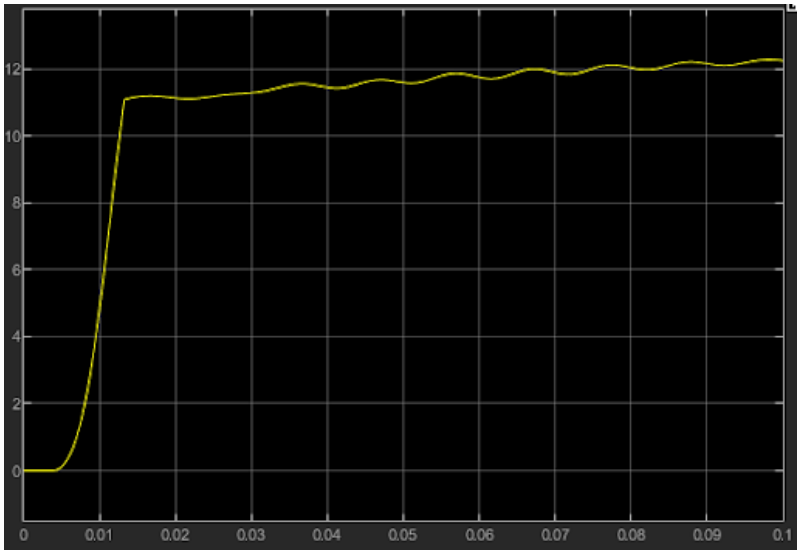

Figure 4.21: Voltage behaviour of the power supply. Vertical axis is voltage (V), horizontal axis is time (s).

After simulating the power supply system, the simulated electrical diagram of the charging system of the battery is presented in Figure 4.22 and the output voltage and current are shown in Figures 4.23 and 4.24, respectively.

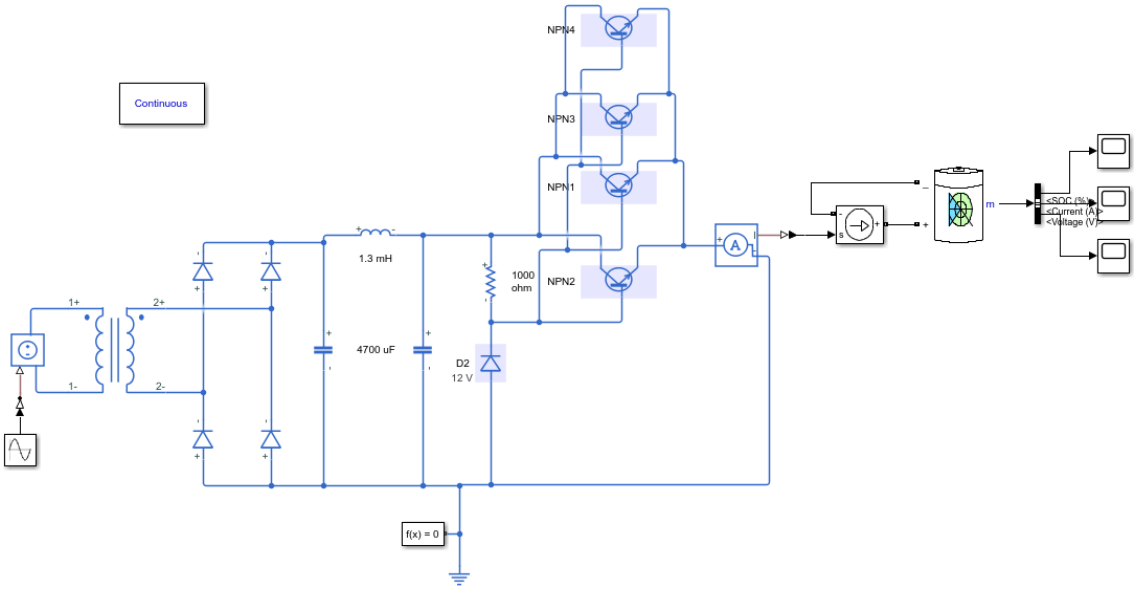

Figure 4.22: Electrical diagram of the developed power supply with current limiter, as implemented in MATLAB/Simulink with Simscape Library.

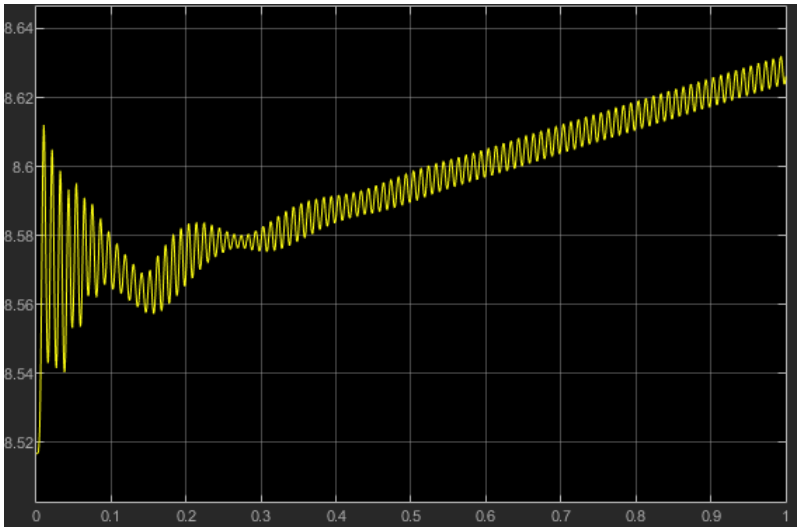

Figure 4.23: Voltage behaviour of the battery with the power supply. Vertical axis is voltage (V), horizontal axis is time (s).

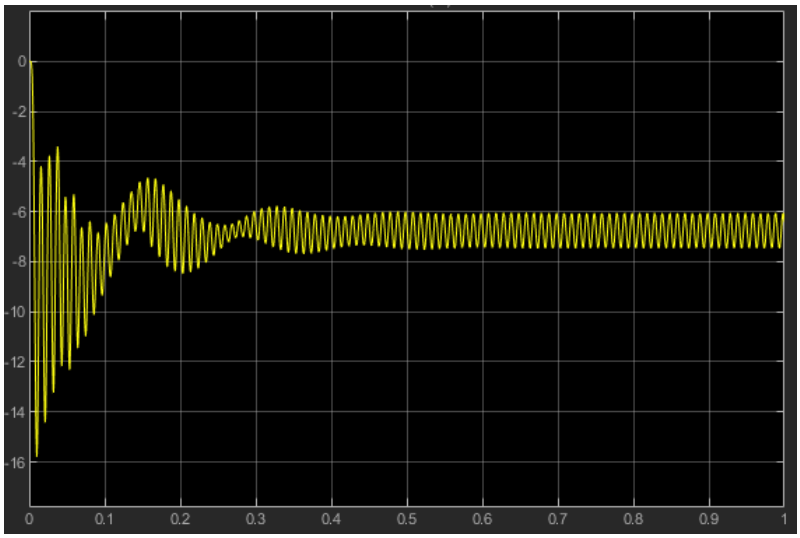

Figure 4.24: Current behaviour of the battery with the power supply. Vertical axis is current (A), horizontal axis is time (s).

4.1.6 Wireless Power Transfer

In order to simulate the operation of a wireless power transfer system, the equivalent circuit of Figure 4.25 was used.

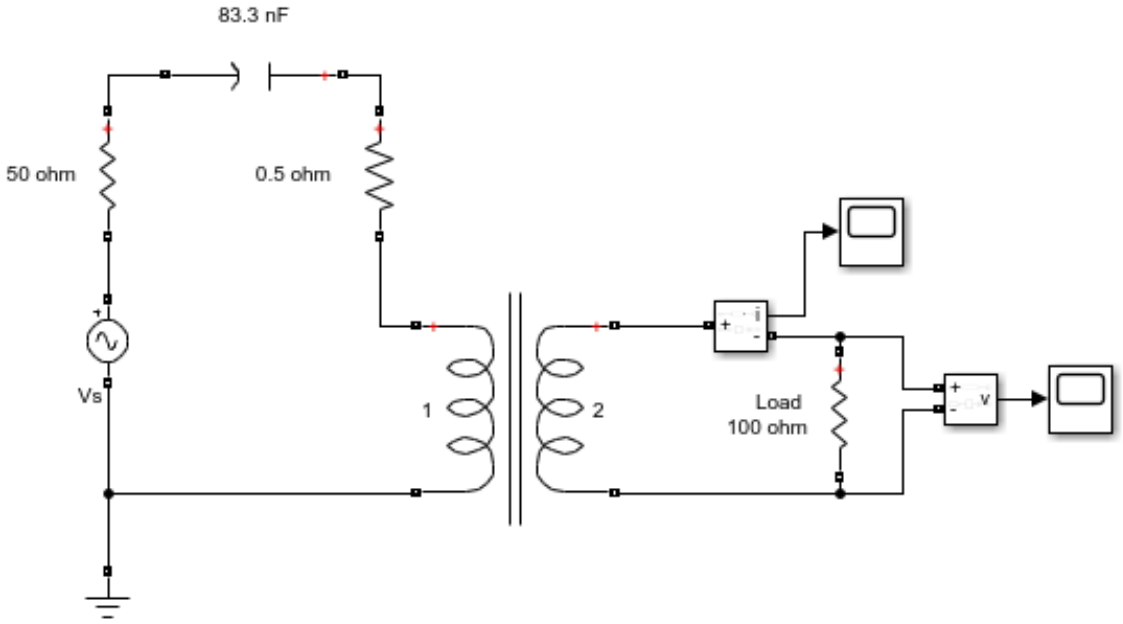

Figure 4.25: Electrical diagram of the developed inductive power transfer simulation, as implemented in MATLAB/Simulink.

First the value of the capacitor is determined for a frequency of 40 kHz and an inductance of the two coils of 1,9 mH using the equation (3.3), so that C_1 = 83,3 nF.

The mutual inductance behaviour with the variation of the distance between the coils is represented in Figure 4.26.

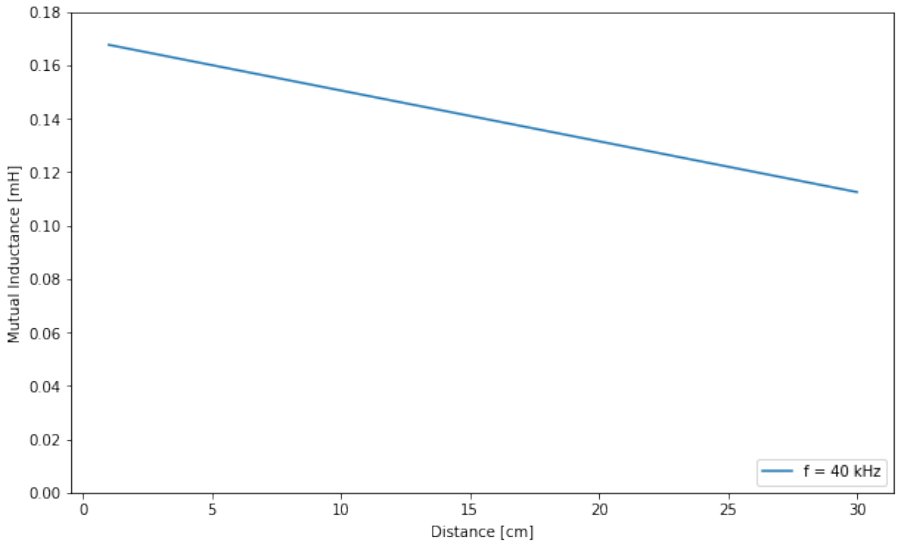

Figure 4.26: Mutual inductance behaviour with variable distance on an inductive power transfer.

From equation (3.10) the efficiency of the system can be obtained with the variation of the distance between the two coils, as is presented in Figure 4.27.

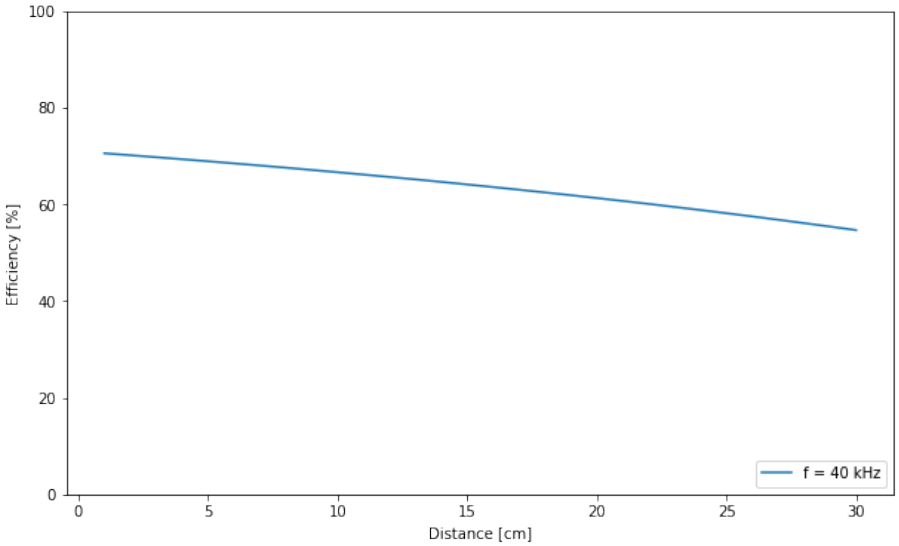

Figure 4.27: Efficiency behaviour with variable distance on an inductive power transfer.

The value of the load resistance R_L can also be varied for a fixed value of the coil's inductance, and is presented in Figures 4.28 and 4.29 its voltage and current behaviour, respectively.

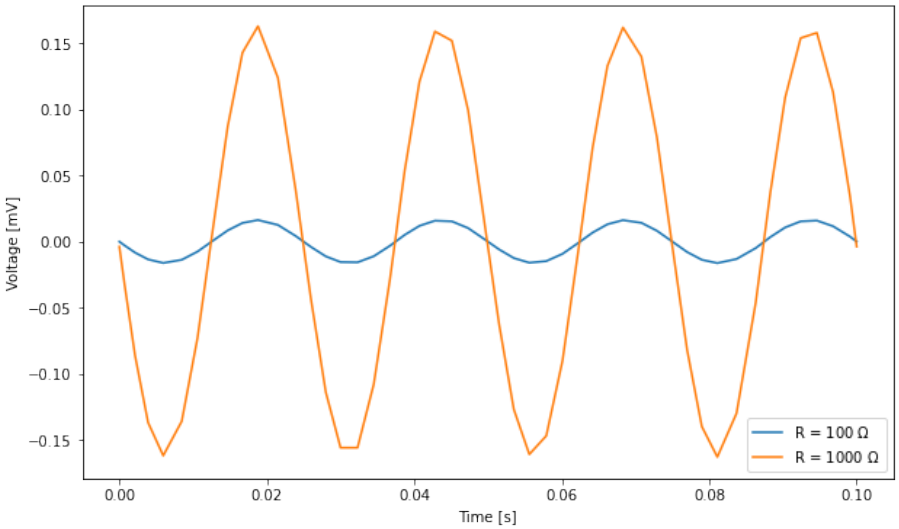

Figure 4.28: Voltage behaviour with variable load resistance on an inductive power transfer.

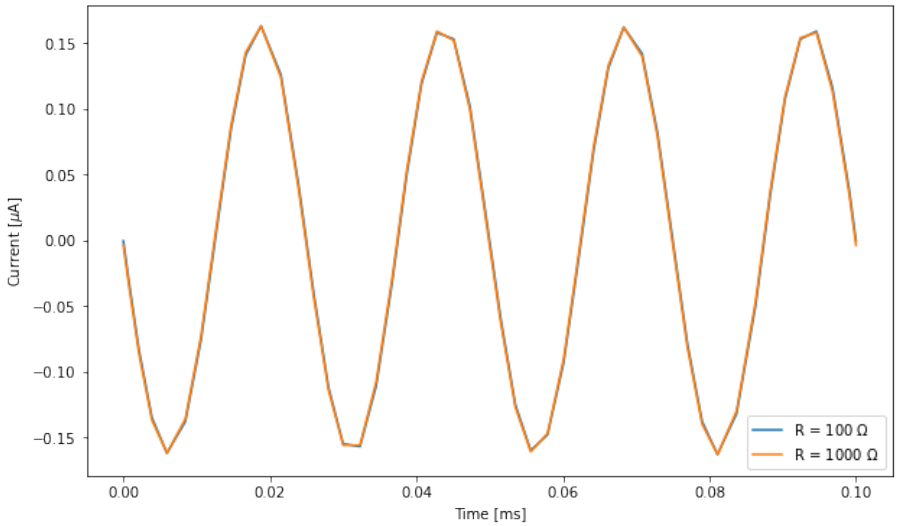

Figure 4.29: Current behaviour with variable load resistance on an inductive power transfer.

From (Mendes, 2021) the coil's inductance was studied when the frequency of the system was varied. Table 4.2 shows the values obtained for different frequencies.

Table 4.2: Inductance values obtained for different frequencies (Mendes, 2021).

Frequency [kHz]	**Inductance [mH]**
20	1,6504
30	1,6421
40	1,6419
50	1,6373
60	1,6322

Figures 4.30 and 4.31 show the obtained voltage and current for the wireless power transfer system.

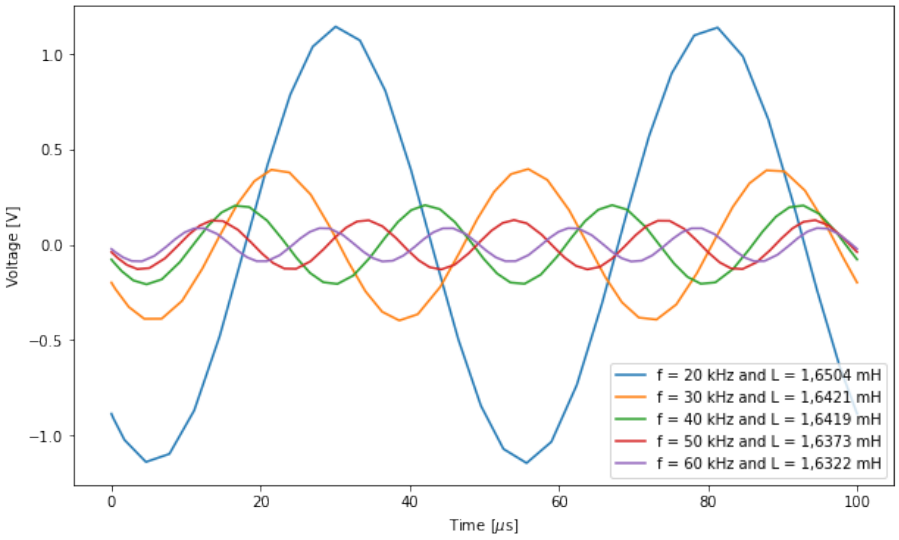

Figure 4.30: Voltage behaviour of the inductive power transfer system with variable frequency and inductance.

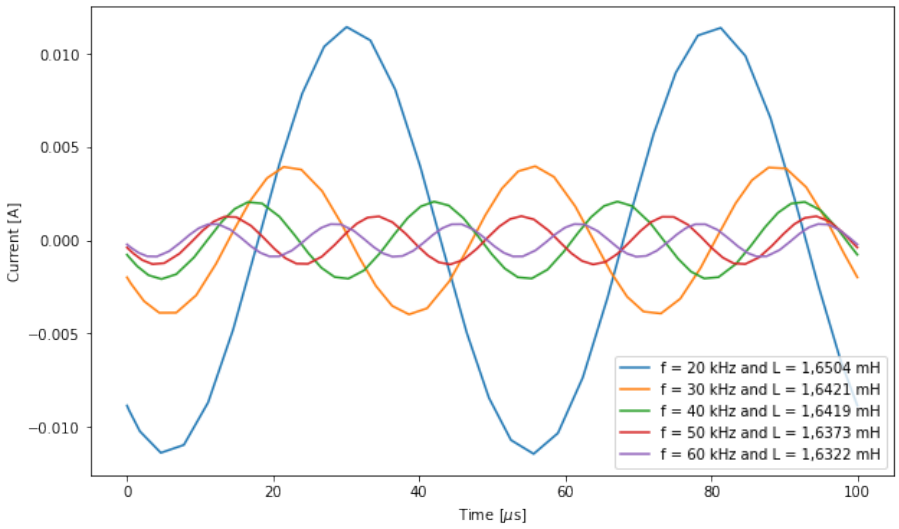

Figure 4.31: Current behaviour of the inductive power transfer system with variable frequency and inductance.

After studying the wireless power system, it was added to Figure 4.22 the system created in Figure 4.25 with Simscape elements, creating the electrical diagram presented in Figure 4.32.

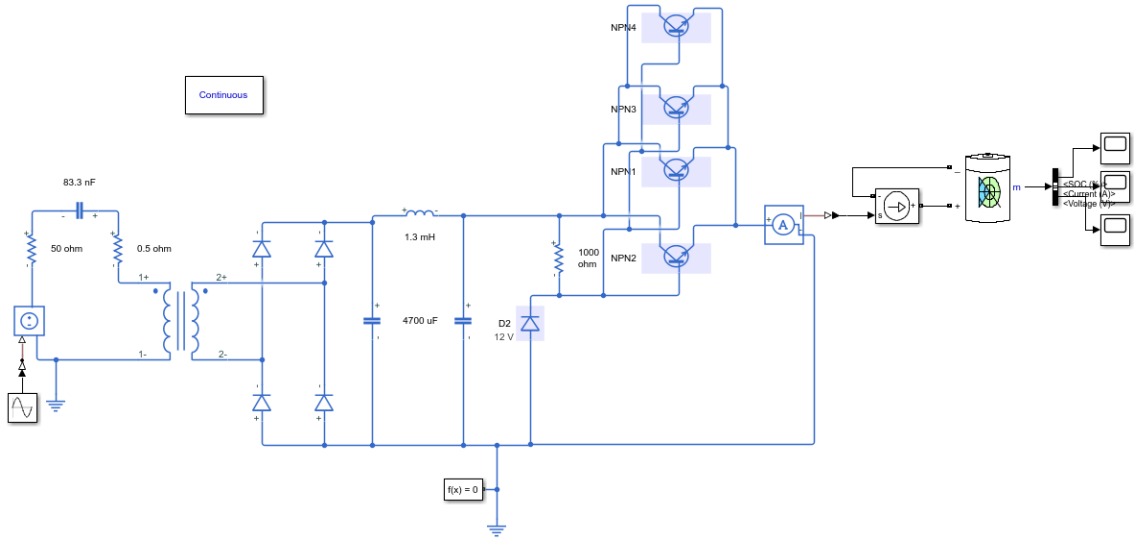

Figure 4.32: Electrical diagram of the developed inductive power transfer with power supply simulation, as implemented in MATLAB/Simulink with Simscape Library.

Figures 4.33 and 4.34 present the voltage and current behaviour of the inductive power transfer with power supply.

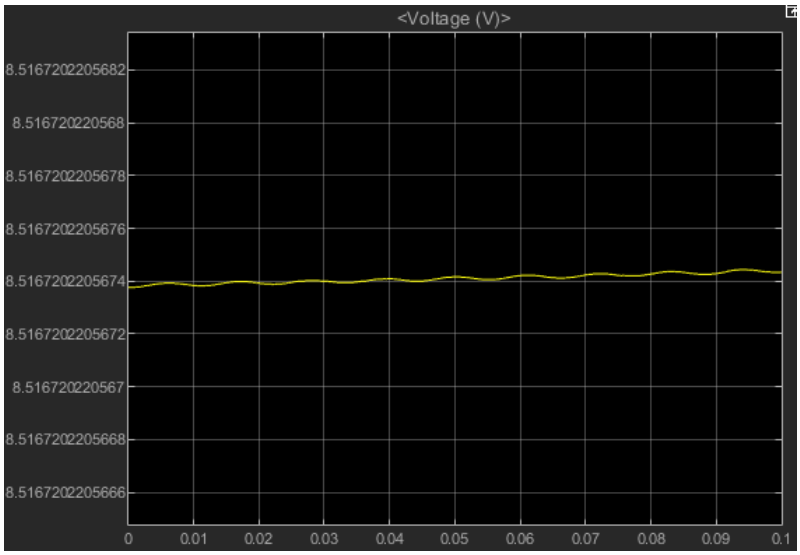

Figure 4.33: Voltage behaviour of the inductive power transfer system with power supply. Vertical axis is voltage (V), horizontal axis is time (s).

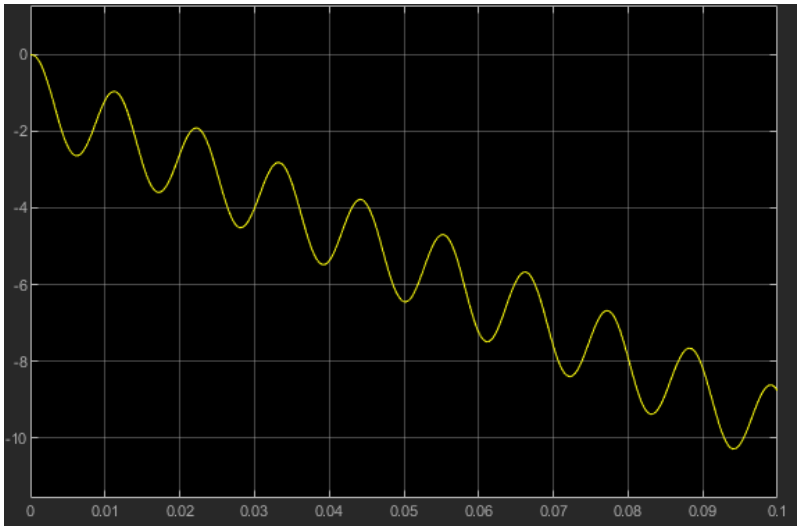

Figure 4.34: Current behaviour of the inductive power transfer system with power supply. Vertical axis is current (A), horizontal axis is time (s).

4.2 Experimental Part

This section presents the experimental procedure and creating of the prototype proposed in the beginning. The first subsection shows the construction of the power supply and tests performed. The second subsection presents the created wireless power transfer system and respective tests.

4.2.1 Power Supply System

As a first version of the prototype of the power supply system, a transformer, full-wave bridge rectifier, capacitor and variable load were connected, as presented in Figure 4.35. The capacitor had a capacitance value of 4700 μF.

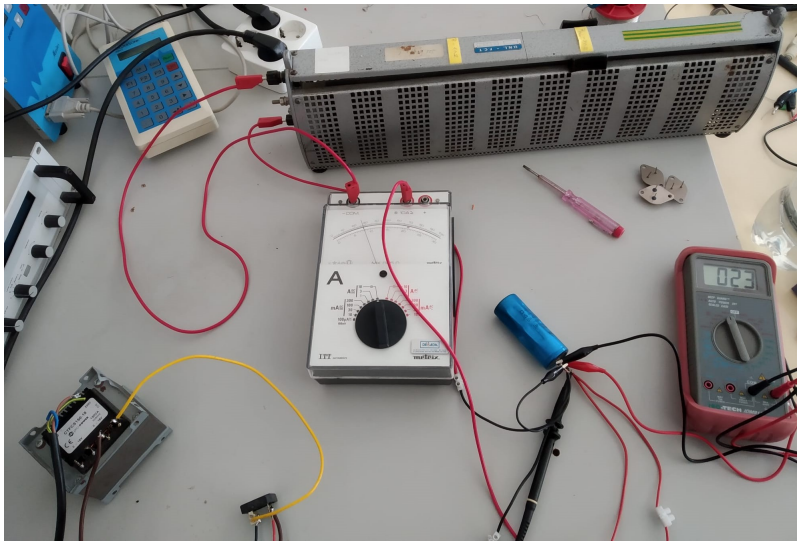

Figure 4.35: First version of the prototype of the power supply system.

First, the capacitor was disconnected in order to verify if the rectification was being done correctly. It started with a load of 12 Ω (Figure 4.36) and then with a load of 8 Ω (Figure 4.37).

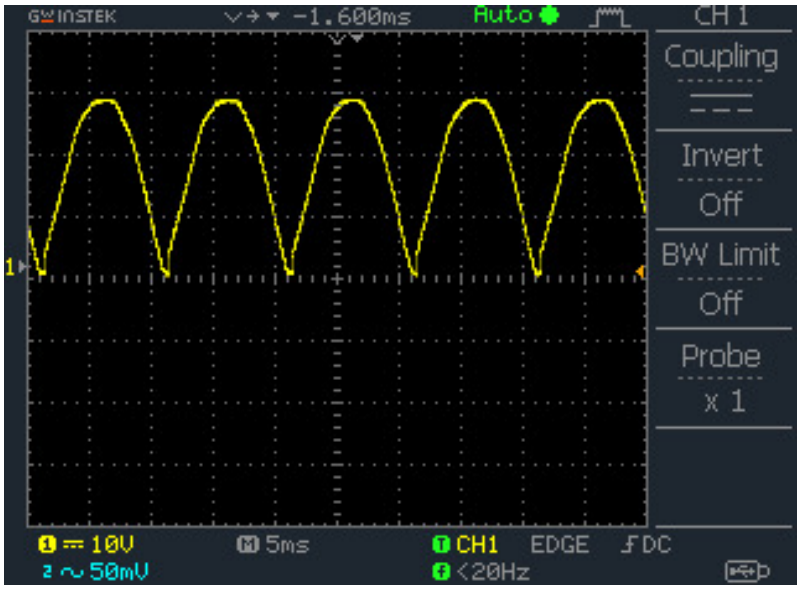

Figure 4.36: Voltage behaviour of the full-wave bridge rectifier with a load of 12 Ω.

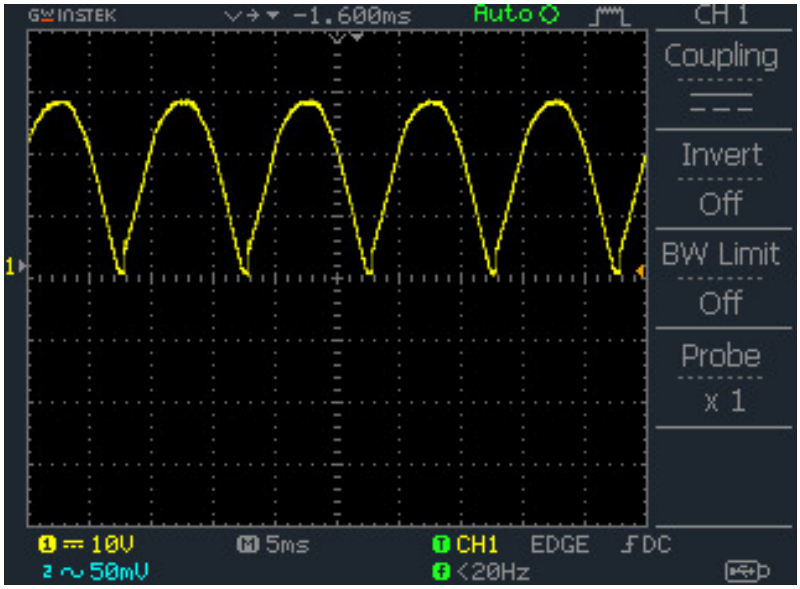

Figure 4.37: Voltage behaviour of the full-wave bridge rectifier with a load of 8 Ω.

The output current and voltage for the two values of the load were measured and are shown in Table 4.3.

Table 4.3: Measured voltage and current of the full-wave bridge rectifier.

Resistance [Ω]	**Voltage [V]**	**Current [A]**
12	13,5	1
8	10,2	1,1

After this the capacitor was reconnected to the system and its output voltage was observed with a load first of 12 Ω (Figure 4.38), then 8 Ω (Figure 4.39), and finally 4 Ω (Figure 4.40).

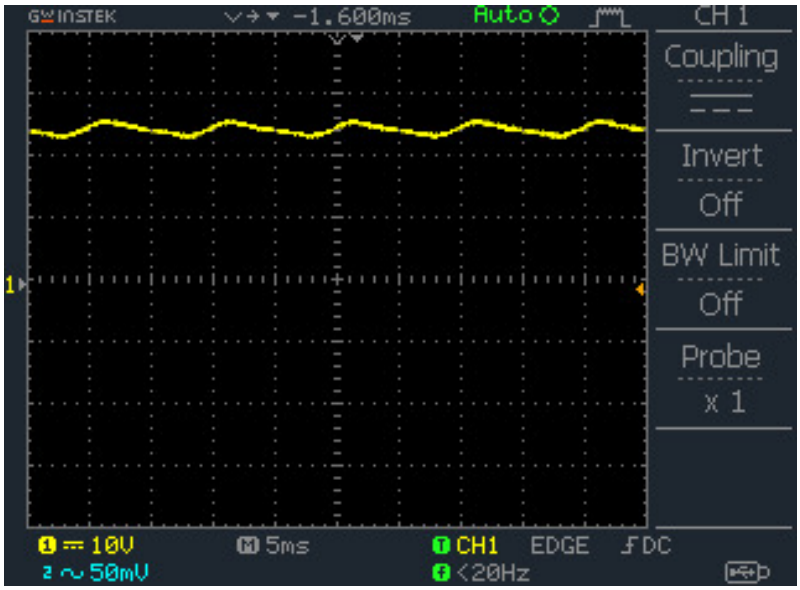

Figure 4.38: Voltage behaviour of the RC filter with a load of 12 Ω.

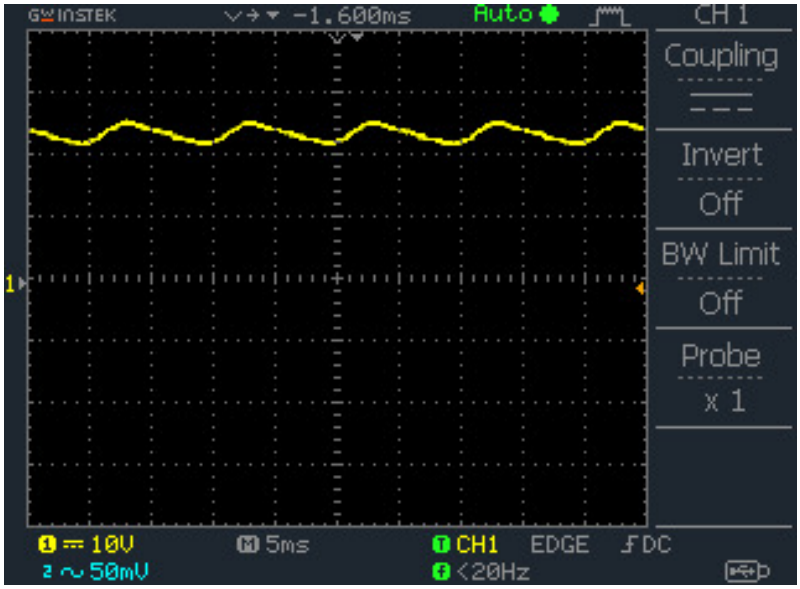

Figure 4.39: Voltage behaviour of the RC filter with a load of 8 Ω.

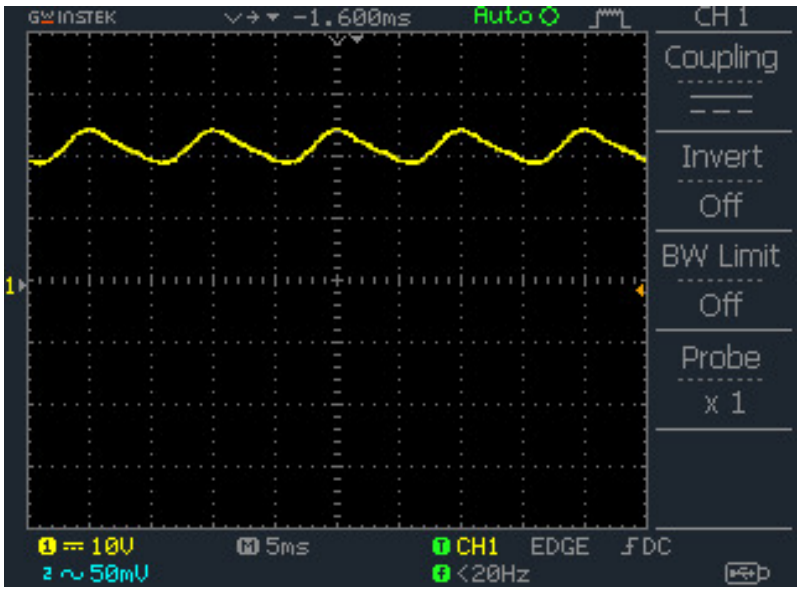

Figure 4.40: Voltage behaviour of the RC filter with a load of 4 Ω.

The output current and voltage for the three different values of the load's resistance were measured and are shown in Table 4.4.

Table 4.4: Measured voltage and current of the RC filter.

Resistance [Ω]	Voltage [V]	Current [A]
12	24,3	1,8
8	23,2	2,7
4	21,3	5

After this the voltage regulator with current limiter and a Pi filter with 4700 μF of capacitance value for the capacitors and 1,3 mH of inductance value for the coil, were added to the circuit of Figure 4.35 thus creating the system presented in Figure 4.41.

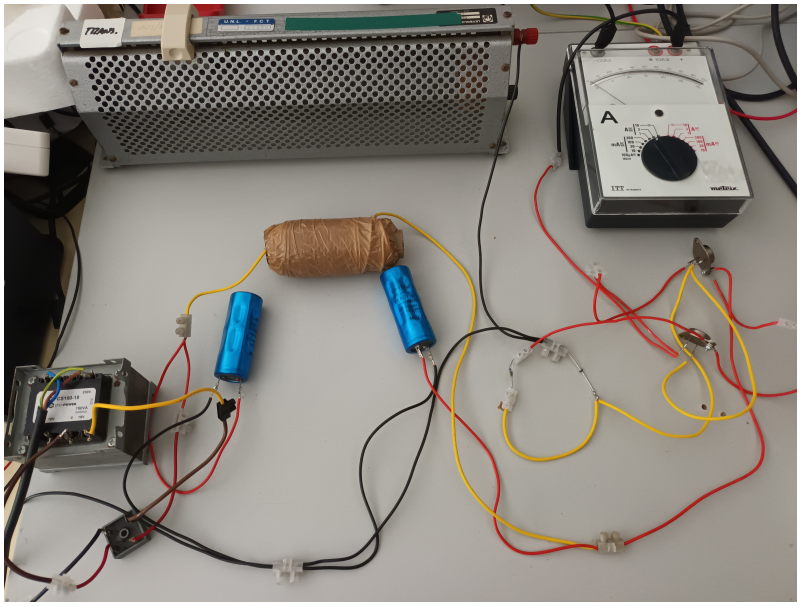

Figure 4.41: Prototype of the power supply system with current limiter.

The output current and voltage for three different load's resistance values were measured and are presented in Table 4.5.

Table 4.5: Measured voltage and current of the power supply system.

Resistance [Ω]	Voltage [V]	Current [A]
12	14	1,2
8	10	1,3
4	5	1,3

4.2.2 Wireless Power Transfer with Superconducting Coils

The used superconducting coils were the ones created in (Mendes, 2021) and one of them is shown in Figure 4.42. The other coil is equal to the presented one.

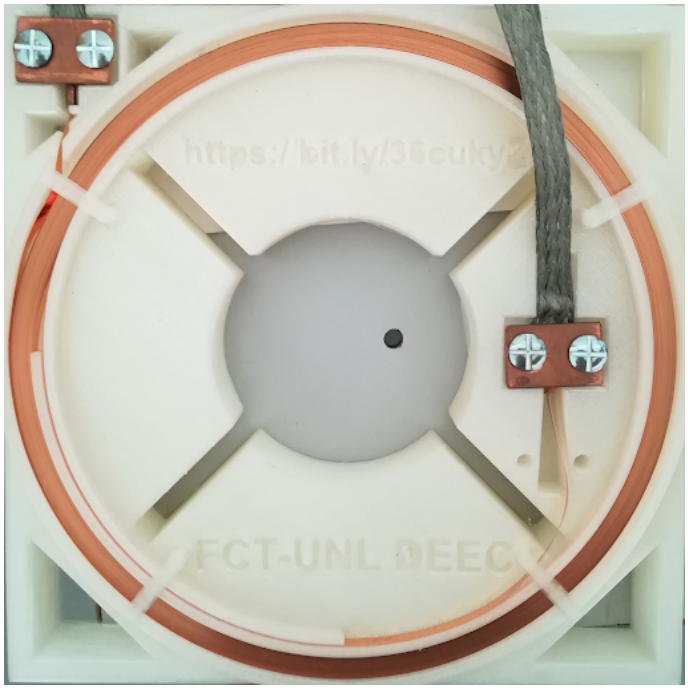

Figure 4.42: Second-generation superconducting tape coil (Mendes, 2021).

The system presented in Figure 4.43 was assembled to allow the receiver coil to be moved, thus changing the distance between the transmitter and receiver.

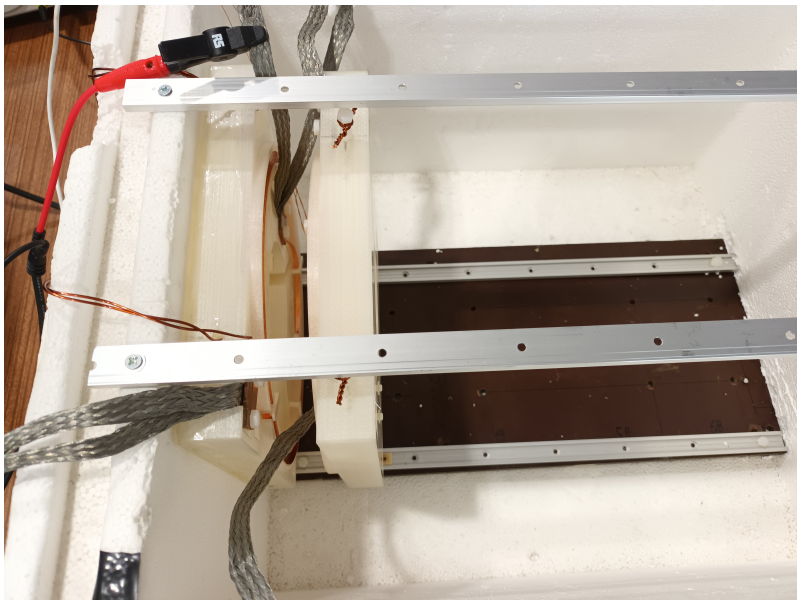

Figure 4.43: Prototype of the wireless power transfer system with the receiver coil close to the emitter one.

Figure 4.44 shows the movement of the receiver coil by increasing the distance between the two coils.

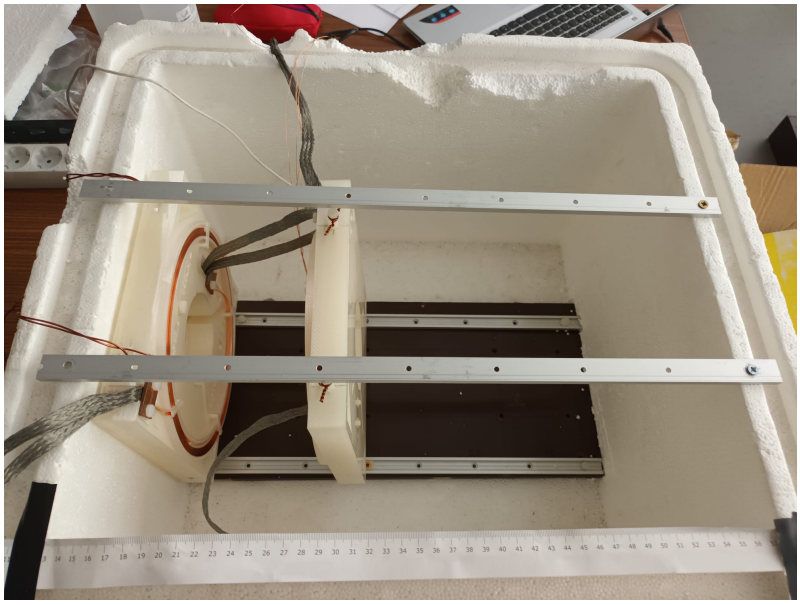

Figure 4.44: Prototype of the wireless power transfer system with the receiver coil away from the emitter one.

In order to have the system working in its resonant frequency it was necessary to add a capacitor in the primary circuit. As it is intended to obtain the highest possible current values, which imply higher values of field density, and in turn a better efficiency, will be considered the test in which the capacitor is added in series with the primary coil, as shown in Figure 4.45.

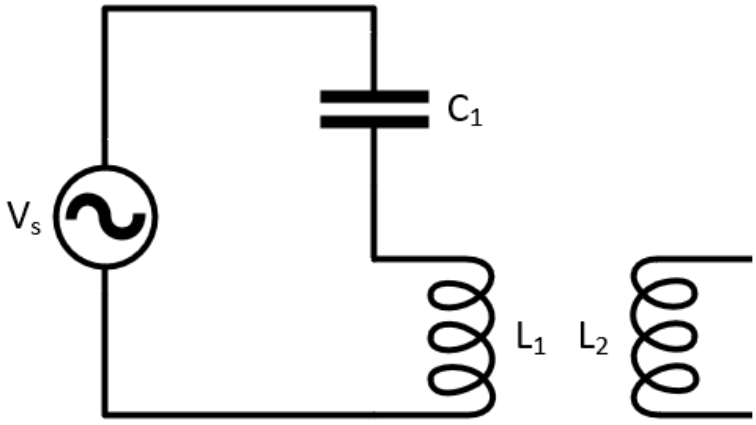

Figure 4.45: Schematic diagram of the wireless power transfer system with a capacitor in series.

It was chosen a capacitor with 150 nF of capacitance. According to equation (3.11) the resonant frequency for that capacitor is 11,07 kHz.

The transmitter coil was connected to a signal generator and according to equation (3.5) in order to calculate the mutual inductance between the coils it is necessary to read the transmitter's current and the voltage of the open-circuit receiver. Figures 4.46 and 4.47 present the primary and secondary circuit output waves, respectively.

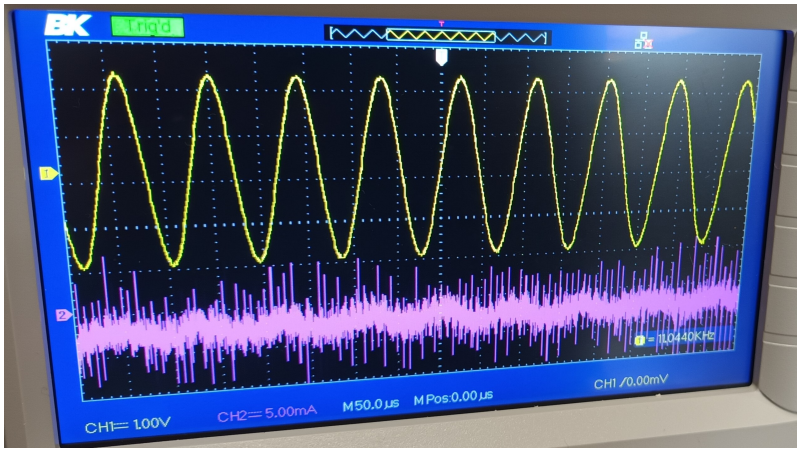

Figure 4.46: Voltage (yellow) and current (pink) behaviour of the primary circuit.

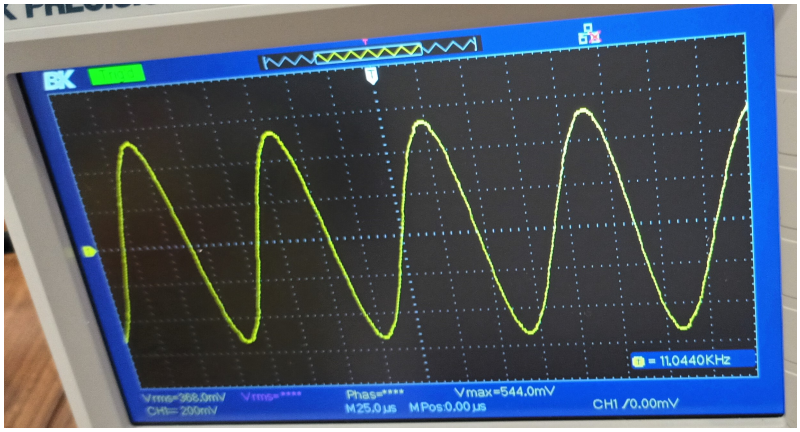

Figure 4.47: Voltage behaviour of the secondary circuit.

Table 4.6 shows the obtained open-circuit voltage values when varying the distance between the coils for the resonant frequency. The primary current throughout the experiment was constant and equal to 2 A.

Table 4.6: Measured open-circuit voltage of the wireless power transfer for the resonant frequency.

d [cm]	U_{OC} **[mV]**
2	680
3	554
4	464
5	408
6	336
7	312
8	264
9	224
10	192
12	168
14	144
16	120
18	96
20	80
22	64
24	50
26	44
28	34
30	30

From Table 4.6 and equation (3.5) the mutual inductance between the coils with variable distance was obtained and is presented in Figure 4.48.

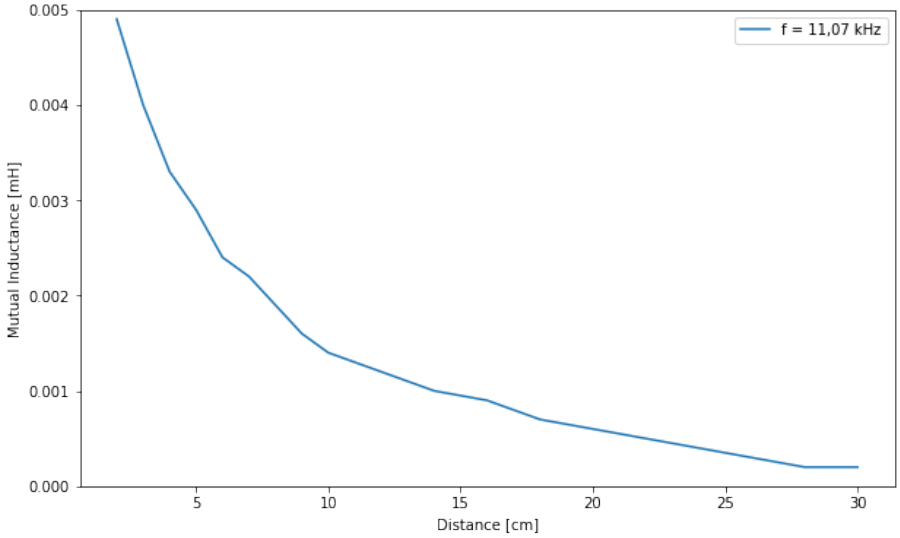

Figure 4.48: Mutual inductance behaviour with variable distance on the constructed wireless power transfer system.

Using the "tendency line" tool from Excel it was given an approximate equation for the graphic obtained in Figure 4.48. Since it has a behaviour close to an exponential the obtained equation was

$$d = 0,0048 \cdot e^{-0,107 \cdot M_{12}}. \tag{4.1}$$

From equation (3.3) the coupling factor between the two coils for variable distances can also be calculated, being presented in Figure 4.49 the obtained graphic.

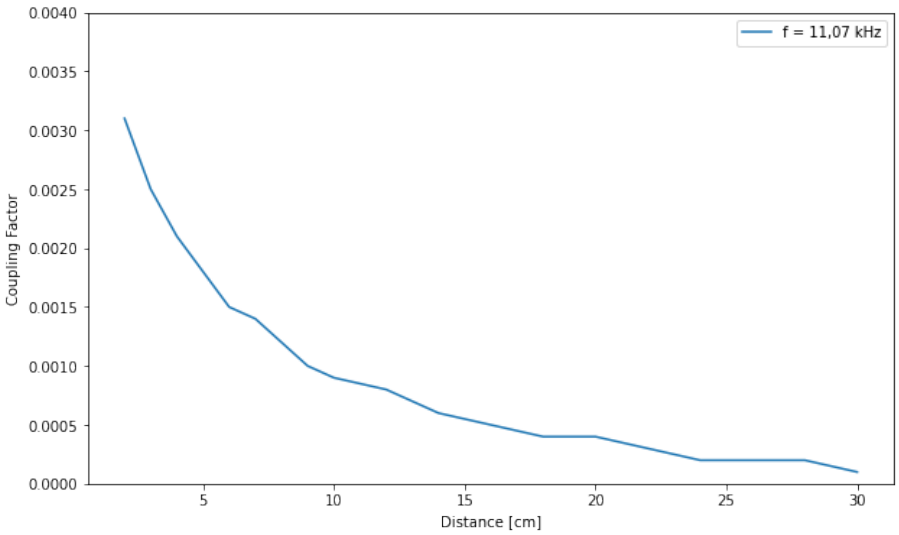

Figure 4.49: Coupling factor behaviour with variable distance on the constructed wireless power transfer system.

4.2.3 Chapter Summary

In this chapter, the simulations necessary for the subsequent construction of the proposed prototype were presented, as well as the experimental version of the wireless power transfer system with a power supply.

MATLAB simulations of all components of a power supply system and the simulations of the operation of a contactless energy transfer system were presented, which allows to conclude that the higher the working frequency, the higher the output voltage and, subsequently, higher system performance.

The experimental procedure and results obtained for the created power supply and wireless power transfer systems were presented.

5

Results Analysis

In this chapter, the results obtained in the simulations carried out in MATLAB/Simulink and those obtained experimentally in the performed tests on the built prototype are analysed and interpreted.

5.1 Simulations

5.1.1 Battery

When analysing Figure 4.3 it can be concluded that the voltage of the Simscape's battery model has an exponential behaviour, and as the voltage increases so does the State-of-Charge of the battery, being completely charged, which means SoC = 100% (Figure 4.2), with a voltage of 16 V (Figure 4.3) when injected with a current of 20 A.

From Figure 4.5 it can be observed that the current of the used battery model with controlled voltage has an exponential behaviour and also decreases with the increase of time, stabilising at 2,5 A.

5.1.2 Rectifier

From Figure 4.8 the rectification of the wave of Figure 4.7 is well performed with a bridge of four diodes, having the negative part of the wave transported to the positive part.

5.1.3 Filter

When it comes to choosing the best filter for the power supply the voltage ripple is the variable that needs to be taken in consideration. From equation (2.5) and Figure 4.11 it can be seen that with the RC filter the voltage ripple is equal to 75 V.

From Figure 4.14 the voltage ripple of the Pi filter is equal to 45 V. This means that a filter with two capacitors and an inductor provides a lower ripple factor, i.e. the ratio of voltage due to AC ripple and direct voltage is lower than the one a filter with one capacitor gives, which means that provides an improved filtering action.

5.1.4 Voltage Regulator

As previously explained in subsection 4.1.4 it was chosen that the voltage regulator would be composed of four NPN transistors in order to limit its output current. With this number of transistors the voltage output is constant and equal to 16 V (Figure 4.17) and the current is subsequently limited to 1,6 A (Figure 4.18) due to the load resistance being equal to 10 Ω.

5.1.5 Power Supply

When creating the complete power supply system and connecting its output to the Simscape's battery model it was obtained in Figure 4.21 a voltage output of approximately 8,6 V and from Figure 4.22 it can be seen that the current was limited to -7 A. The current has a negative signal due to the battery being charged, i.e. the current is flowing from the power supply to the battery.

5.1.6 Wireless Power Transfer

When examining Figures 4.26 and 4.27 it can be observed that the higher the distance between the receiver and transmitter coils the lower its mutual inductance and system efficiency for a fixed frequency, which was expected from the Wireless Power Transfer's theory presented in section 2.1.

When varying the value of the load resistance (Figure 4.28) the higher the output voltage of the system, which is in accordance with Ohm's Law.

From Table 4.2 it is taken that the higher the work frequency the lower the coil's inductance. And by observing Figures 4.30 and 4.31 it can be concluded that with higher frequency also comes lower output voltage and current.

When connecting the previously created power supply to the wireless power transfer system it was observed in Figure 4.33 that the output voltage of the system is constant and equal to 8,5 V. In Figure 4.34 the current is limited to -10 A. This means that when adding the power supply the complete system works as intended.

5.2 Laboratory Tests

5.2.1 Power Supply

In order to check if by simulating the system constructed in Figure 4.35 the output values were the same as the ones obtained experimentally, a schematic equal to the one in Figure 4.10 was designed in MATLAB/Simulink with a load of 12 Ω and its output voltage and current were observed, as presented in Figures 5.1 and 5.2, respectively.

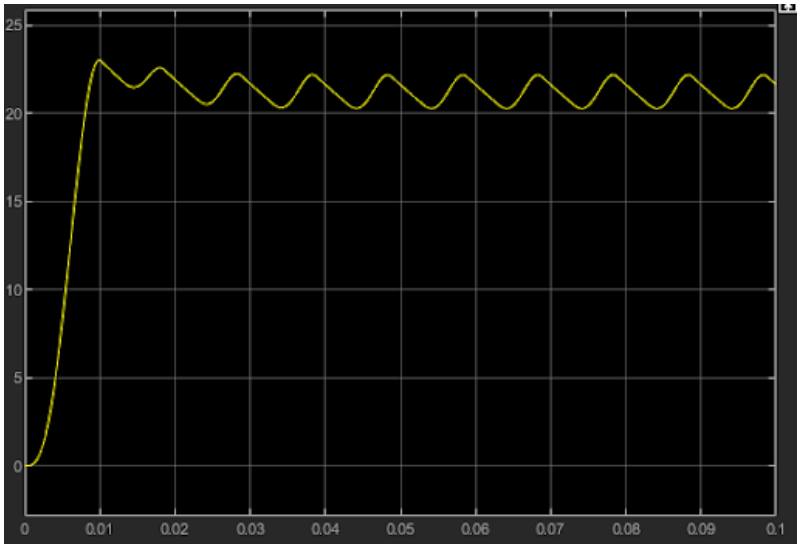

Figure 5.1: Voltage behaviour of the full-wave bridge rectifier with an RC filter and load of 12 Ω. Vertical axis is voltage (V), horizontal axis is time (s).

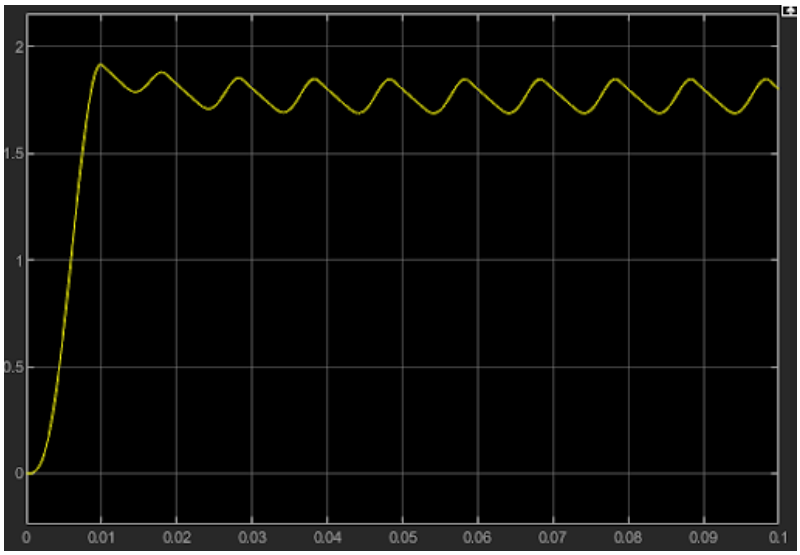

Figure 5.2: Current behaviour of the full-wave bridge rectifier with an RC filter and load of 12 Ω. Vertical axis is current (A), horizontal axis is time (s).

From Figures 5.1 and 5.2 it can be seen that for a load of 12 Ω the output voltage reaches approximately 23 V and the current reaches almost 2 A. From Table 4.4 and for a load of 12 Ω it was obtained a voltage of 24,3 V and current of 1,8 A, which is very similar to the values obtained per simulation.

The same can be done for the constructed power supply by simulating the schematic from Figure 4.19 in MATLAB/Simulink with a load of 12 Ω. Figures 5.3 and 5.4 present the obtained voltage and current, respectively.

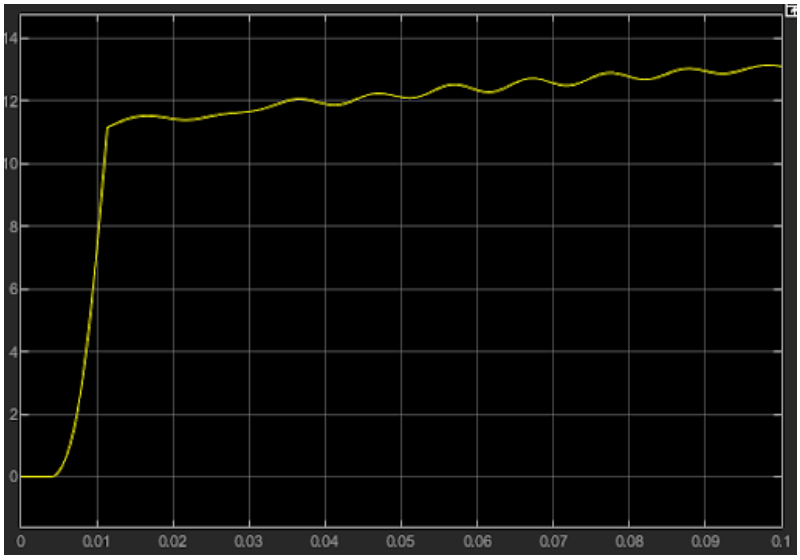

Figure 5.3: Voltage behaviour of the power supply with a load of 12 Ω. Vertical axis is voltage (V), horizontal axis is time (s).

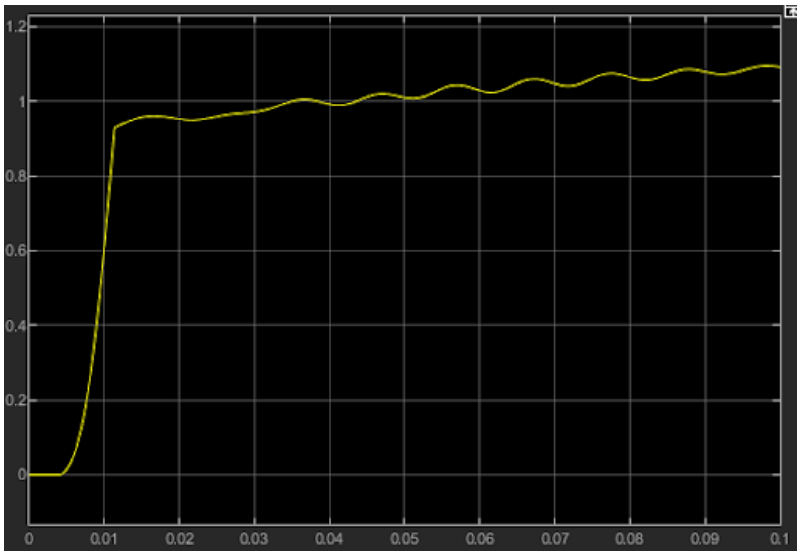

Figure 5.4: Current behaviour of the power supply with a load of 12 Ω. Vertical axis is current (A), horizontal axis is time (s).

From Figures 5.3 and 5.4 it is observed that for a load of 12 Ω the power supply reaches a voltage of 13 V and a current of 1,1 A. From Table 4.5 the constructed power supply reaches 14 V and 1,1 A for the same load, which is similar to the values obtained through simulation. It can also be seen that the current becomes almost constant both in the simulation and experimentally, due to the current limiter.

5.2.2 Wireless Power Transfer

In resonant systems it is possible to get maximum values of current, with a series circuit, or maximum values of voltage, with a parallel circuit. For the constructed wireless power

system the additional capacitor was placed in series with the transmitter coil, which allows for a bigger efficiency due to the maximum values of current that can be seen in Figure 4.46. With maximum values of current there will be bigger magnetic field density values, which leads to a better coupling between the transmitter and receiver coils.

From Table 4.6 it can be inferred that the bigger the distance between the two coils the lower the open-circuit voltage on the secondary circuit, and from Figures 4.48 and 4.49 it's seen that with the higher the distance the lower the mutual inductance will be and the same happens to the coupling factor, which is in accordance with what was previously mentioned in Chapter 2.

5.3 Chapter Summary

This chapter presents the analysis of the results obtained in the simulations carried out in MATLAB/Simulink and in the tests carried out in the laboratory of the prototypes built.

It was shown that for the construction of a power supply in which it is possible to regulate the voltage and limit the output current, several NPN transistors are needed after filtering, and from five transistors the differences are very small, so there is no practical advantage of using more than four.

It was also shown that the results obtained in the simulations and in the laboratory of the power supply are similar, so the system created in simulation is suitable for the simulation of a real system and allows it to be dimensioned prior to its practical construction.

The results obtained for the built-in contactless energy transfer system were also presented, where it was possible to verify that the mutual inductance between the transmitting and receiving coils decreases considerably with increasing distance between them, which, in turn, will reduce the system efficiency when having power transmission.

The following chapter will present the main conclusions reached and the future work that will be convenient and necessary to carry out.

6

Conclusions and Future Work

This chapter presents the main conclusions obtained after the completion of this work. However, this subject does not end with this contribution, so suggestions for future work are also presented.

6.1 Conclusions

Throughout this dissertation, the steps to be taken in the design of a power transfer system without contact with a power supply as an output unit were presented in order to power a lead acid battery, using two superconducting coils, one in the transmission circuit and the other in the receiving circuit.

First, the MATLAB/Simulink tool was used in conjunction with the Simscape library to perform electrical simulations of the various system components. They separated into two systems in order to better understand the functioning of each individual: the power supply and the transfer of contactless energy.

In the simulations of the power supply, grinding and filtering were studied, using a complete wave bridge rectifier and a Pi filter consisting of two condensers in parallel with a coil. In addition, we sought to build a source that functioned as a current limiter and a voltage regulator. To this end, we studied the number of NPN transistors in series that would be needed, and it was concluded that from five the differences were minimal, so it was chosen to use four.

Regarding the simulations of the contactless energy transfer system, the effect of the variation of the distance between the transmitting and receiver coils on the mutual inductance of the coils to a fixed frequency was first studied, verifying that the greater the distance the lower the mutual inductance. Then the same simulation was performed but observing what happens to the efficiency of the system, verifying that the greater the distance, the lower the efficiency.

Then, the effect of frequency variation between the transmitter and receiver coils was studied, verifying that the higher the frequency, the higher the voltage and output current.

Having the individual simulations performed, a simulation was carried out with the

complete system charging a lead acid battery. Here it was possible to conclude that the system created is able to charge the battery and limit the current that reaches it so as not to overload it.

After these simulations, the prototype of the system was constructed, starting with the construction of the power supply, where the constructed source was tested and the MATLAB/Simulink was reused to compare the results obtained experimentally with those obtained by simulation and it was verified that they were quite similar.

Then, the energy transfer system was built where care was taken to create a system that allowed the horizontal movement of the transmitting and receiver coils. With the aid of a condenser in the transmission circuit, the system was sought to have the system in the resonance frequency with the reception circuit open, having used a signal generator to inject a sinusoidal wave into the transmitting circuit. Finally, it was possible to test the effect of the variation of the distance between the coils in the mutual inductance, verifying that the greater the distance the smaller the mutual inductance, having a behaviour similar to an exponential.

6.2 Future Work

Based on the results obtained throughout the dissertation, some ways to continue and improve the developed contactless energy transfer system can be found.

A step to be taken next would be to replace the signal generator used by a source capable of providing reasonable voltage and current values in order to be able to analyse the behaviour of the contactless power transfer system implemented with considerable power. With this source it would be possible to verify the effect of the variation of the distance between the coils on the efficiency of the system.

Another future work would be to connect the built-in power supply to the output of the contactless power transfer receiver circuit and its connection to the lead acid battery obtained in order to experimentally verify whether the built prototype would be able to charge the battery at considerable distances between the coils.

Bibliography

Amaral, A., & Cardoso, A. (2016). Voltage Doubler for AC-DC Step-up Linear Power Supplies: Design, Modelling and Simulation. *Acta Electrotechnica et Informatica*, *16*(4), 3–10. https://doi.org/10.15546/aeei-2016-0025

Barman, S. D., Reza, A. W., Kumar, N., Karim, M. E., & Munir, A. B. (2015). Wireless powering by magnetic resonant coupling: Recent trends in wireless power transfer system and its applications. *Renewable and Sustainable Energy Reviews*, *51*, 1525–1552. https://doi.org/10.1016/j.rser.2015.07.031

Bhutkar, R., & Sapre, S. (2009). Wireless energy transfer using magnetic resonance. *2009 Second International Conference on Computer and Electrical Engineering*, *1*, 512–515. https://doi.org/10.1109/ICCEE.2009.194

Bi, Z., Kan, T., Mi, C. C., Zhang, Y., Zhao, Z., & Keoleian, G. A. (2016). A review of wireless power transfer for electric vehicles: Prospects to enhance sustainable mobility. *Applied Energy*, *179*, 413–425. https://doi.org/10.1016/j.apenergy.2016.07.003

Brown, W., Mims, J., & Heenan, N. (1965). An experimental microwave-powered helicopter. *1958 IRE International Convention Record*, *13*, 225–235. https://doi.org/10.1109/IRECON.1965.1147518

Brown, W. (1984). The history of power transmission by radio waves. *IEEE Transactions on Microwave Theory and Techniques*, *32*(9), 1230–1242. https://doi.org/10.1109/TMTT.1984.1132833

Budhia, M., Boys, J. T., Covic, G. A., & Huang, C.-Y. (2013). Development of a single-sided flux magnetic coupler for electric vehicle ipt charging systems. *IEEE Transactions on Industrial Electronics*, *60*(1), 318–328. https://doi.org/10.1109/TIE.2011.2179274

Chernoplekov, N. A. (2002). State of the art in applied high-current superconductivity. *Physics-Uspekhi*, *45*(6), 659–665. https://doi.org/10.1070/pu2002v045n06abeh001198

Faruk, B. M., Jawarkar, U. S., Pal, T. G., & Gugliya, A. S. (2017). Wireless Power Transfer Electric Vehicle. *International Advanced Research Journal in Science, Engineering and Technology*, *4*(4), 111–119. https://doi.org/10.17148/IARJSET

Hu, B., Li, H., Li, T., Wang, H., Zhou, Y., Zhao, X., Hu, X., Du, X., Zhao, Y., Li, X., Qi, T., Helaoui, M., Chen, W., & Ghannouchi, F. (2021). A long-distance high-power microwave wireless power transmission system based on asymmetrical resonant magnetron and cyclotron-wave rectifier. *Energy Reports*, *7*, 1154–1161. https://doi.org/10.1016/j.egyr.2020.12.026

Jeong, I.-S., Choi, H.-S., & Chung, D.-C. (2017). Analysis of reflection-coefficient by wireless power transmission using superconducting coils. *Progress in Superconductivity and Cryogenics (PSAC)*, *19*, 29–32. https://doi.org/10.9714/psac.2017.19.2.029

Jones, M. (2012). Power Supplies. *Valve Amplifiers*, 333–434. https://doi.org/10.1016/b978-0-08-096640-3.00005-8

Kalwar, K. A., Aamir, M., & Mekhilef, S. (2015). Inductively coupled power transfer (ICPT) for electric vehicle charging – A review. *Renewable and Sustainable Energy Reviews*, *47*, 462–475. https://doi.org/10.1016/j.rser.2015.03.040

Khang, S.-T., Lee, D.-J., Hwang, I.-J., Yeo, T.-D., & Yu, J.-W. (2018). Microwave Power Transfer With Optimal Number of Rectenna Arrays for Midrange Applications. *IEEE Antennas and Wireless Propagation Letters*, *17*(1), 155–159. https://doi.org/10.1109/lawp.2017.2778507

Khutwad, S. R., & Gaur, S. (2016). Wireless charging system for electric vehicle. *2016 International Conference on Signal Processing, Communication, Power and Embedded System (SCOPES)*, 441–445. https://doi.org/10.1109/SCOPES.2016.7955869

Kinsky, G. (2021). Android Phones with Wireless Charging. https://powermat.com/blog/android-wireless-charging/

Lourenço, J. M. (2021). *The NOVAthesis LaTeX Template User's Manual*. NOVA University Lisbon. https://github.com/joaomlourenco/novathesis/raw/master/template.pdf

Lu, X., Niyato, D., Wang, P., & Kim, D. I. (2015). Wireless charger networking for mobile devices: fundamentals, standards, and applications. *IEEE Wireless Communications*, *22*(2), 126–135. https://doi.org/10.1109/mwc.2015.7096295

Lu, X., Wang, P., Niyato, D., Kim, D. I., & Han, Z. (2016). Wireless charging technologies: Fundamentals, standards, and network applications. *IEEE Communications Surveys Tutorials*, *18*(2), 1413–1452. https://doi.org/10.1109/COMST.2015.2499783

MA, Y. (2004). Second generation YBCO coated conductors: A review. *Chinese Science Bulletin*, *49*(23), 24–35. https://doi.org/10.1360/04we0094

Machura, P., Zhang, H., Kails, K., & Li, Q. (2020). Loss characteristics of superconducting pancake, solenoid and spiral coils for wireless power transfer. *Superconductor Science and Technology*, *33*(7), 074008. https://doi.org/10.1088/1361-6668/ab931d

Maxwell, J. C. (1873). *A treatise on electricity and magnetism*.

Mendes, C. A. (2021). *Sistema de Transferência de Energia sem Contacto para um Comboio de Levitação Magnética (MagLev) real: aplicação ao Cobra* (tech. rep. Masters Dissertation). FCT-UNL.

Mohammed, S. S., Ramasamy, K., & Shanmuganantham, T. (2010). Wireless Power Transmission - A Next Generation Power Transmission System. *International Journal of Computer Applications*, *1*(13), 102–105. https://doi.org/10.5120/274-434

Mou, X., & Sun, H. (2015). Wireless Power Transfer: Survey and Roadmap. *2015 IEEE 81st Vehicular Technology Conference (VTC Spring)*. https://doi.org/10.1109/vtcspring.2015.7146165

Mourachkine, A. (2004). *Room-temperature Superconductivity*. Cambridge University Press.

Osanlo, M., Pouresmaeil, K., & Kaboli, S. (2020). A Low Loss Linear Voltage Regulator for High Voltage DC Power Supplies Based on Adjustable Inductors. *2020 11th Power Electronics, Drive Systems, and Technologies Conference (PEDSTC)*. https://doi.org/10.1109/pedstc49159.2020.9088388

Plonus, M. (2020). Diode Applications. *Electronics and Communications for Scientists and Engineers*, 121–139. https://doi.org/10.1016/b978-0-12-817008-3.00003-6

Roque, A., Sousa, D., Fernão Pires, V., & Margato, E. (2017). Superconductivity and their Applications. *Renewable Energy and Power Quality Journal*, *1*(15), 322–327. https://doi.org/10.24084/repqj15.308

Schlesak, J., Alden, A., & Ohno, T. (1988). A microwave powered high altitude platform. *1988., IEEE MTT-S International Microwave Symposium Digest*, *1*, 283–286. https://doi.org/10.1109/MWSYM.1988.22031

Shaposhnikov, S. S. (2002). Wireless Power Transmission Antennas: Peculiarities for the Space Power Systems. *Space 2002 and Robotics 2002*. https://doi.org/10.1061/40625(203)33

Sidiku, M., Eronu, E., & Ashigwuike, E. (2021). A review on wireless power transfer: Concepts, implementations, challenges, and mitigation scheme. *Nigerian Journal of Technology*, *39*(4), 1206–1215. https://doi.org/10.4314/njt.v39i4.29

Singh, S. K., Hasarmani, T. S., & Holmukhe, R. M. (2012). Wireless Transmission of Electrical Power Overview of Recent Research Development. *International Journal of Computer and Electrical Engineering*, 207–211. https://doi.org/10.7763/ijcee.2012.v4.480

Solovyeva, E. B., Ezerov, K. S., & Inshakov, Y. M. (2021). Full-Wave Rectification Based on Diode Bridge in NI ELVIS Complex. *2021 International Conference on Quality Management, Transport and Information Security, Information Technologies (ITQMIS)*, 723–727. https://doi.org/10.1109/itqmis53292.2021.9642794

Strassner, B., & Chang, K. (2013). Microwave power transmission: Historical milestones and system components. *Proceedings of the IEEE*, *101*(6), 1379–1396. https://doi.org/10.1109/JPROC.2013.2246132

Thakur, V. V., & Abrol, S. A. (2017). Wireless power transfer applications and its comparison with wired short distance transmission.

Tinkham, M. (2004). *Introduction to Superconductivity* (Second). Dover Publications.

Tremblay, O., Dessaint, L.-A., & Dekkiche, A.-I. (2007). A generic battery model for the dynamic simulation of hybrid electric vehicles. *VPPC 2007 - Proceedings of the 2007*

IEEE Vehicle Power and Propulsion Conference, 284–289. https://doi.org/10.1109/VPPC.2007.4544139

Utschick, C. (2021). *Superconducting wireless power transfer at high power densities for industrial applications and fast battery charging* (Doctoral dissertation). Technische Universität München.

Valtchev, S., Baikova, E., & Jorge, L. (2012). Electromagnetic field as the wireless transporter of energy. *Facta universitatis - series: Electronics and Energetics*, *25*(3), 171–181. https://doi.org/10.2298/fuee1203171v

Waffenschmidt, E. (2011). Wireless power for mobile devices. *2011 IEEE 33rd International Telecommunications Energy Conference (INTELEC)*, 1–9. https://doi.org/10.1109/INTLEC.2011.6099840

Wang, B., Yerazunis, W., & Teo, K. H. (2013). Wireless Power Transfer: Metamaterials and Array of Coupled Resonators. *Proceedings of the IEEE*, *101*(6), 1359–1368. https://doi.org/10.1109/jproc.2013.2245611

Yusop, Y., Saat, S., Husin, H., Nguang, S. K., & Hindustan, I. (2016). Analysis of Class-E LC Capacitive Power Transfer System. *Energy Procedia*, *100*, 287–290. https://doi.org/10.1016/j.egypro.2016.10.179

Zouaoui, S., Dghais, W., Romba, L., Melicio, R., & Belgacem, H. (2022). Integrated wpt-plc system applied to uav: Characterization of a two-coil channel considering misalignment scenarios. *Electronics*, *11*(8). https://doi.org/10.3390/electronics11081249